ATLANTIC TROPICAL CYCLONE FORMATION: PRE-GENESIS EVOLUTION OF TROPICAL EASTERLY WAVES AND IMPACTS OF THE MIDDLE TO UPPER TROPOSPHERIC DRY AIR

BY

ISAAC E. HANKES

DISSERTATION

Submitted in partial fulfillment of the requirements
for the degree of Doctor of Philosophy in Atmospheric Sciences
in the Graduate College of the
University of Illinois at Urbana-Champaign, 2014

Urbana, Illinois

Doctoral Committee:

Assistant Professor Zhuo Wang, Chair
Professor Robert Rauber
Associate Professor Stephen Nesbitt
Doctor Timothy Dunkerton

Abstract

This study first provides an overview of the dynamic and thermodynamic evolution of tropical easterly waves (TEWs) for 164 named tropical storms over the Atlantic during 1989-2010 July-October. The evolution of precipitation and the low-level convergence suggests that convection begins to organize near the center of the wave critical layer about one day prior to genesis, along with the rapid intensification of vorticity. The composites derived from the ERA-Interim reanalysis reveal higher specific humidity and equivalent potential temperature near the center of the wave critical layer, especially in the middle troposphere within one day prior to genesis.

The study then focuses on the formation of the Cape Verde storms over the East Atlantic. There are two groups of easterly waves over West Africa, one to the south and the other to the north of the African Easterly Jet (AEJ), which sometimes merge near the coast of West Africa. Three groups of waves are identified in order to determine the role of wave merger in tropical cyclogenesis over the East Atlantic: non-merger developers, merger developers, and merger non-developers. Relative to non-mergers, it is found that merger developers have a weaker circulation near the surface at the early stages but the merger of a southern wave with a northern wave leads to a stronger and deeper wave pouch, which is more conducive to tropical cyclogenesis. It is also found that dry air intrusion west of the wave trough in the middle and upper troposphere inhibits deep convection and leads to the nondevelopment of some mergers, but that boundary layer dry air in the northern waves moistens quickly over the ocean and does not impede development.

The interannual variability of the middle and upper tropospheric dry air and its impacts on tropical cyclone activity over the Atlantic are further examined using the EOF analysis and composite analysis. It is found that the interannual variability of the upper-tropospheric (300-500 hPa) dry events is to some extent independent of that in the middle troposphere (600-850 hPa), and both have impacts on the interannual variability of Atlantic tropical cyclone activity. The sources of dry air and its association with African dust outbreaks are also examined.

Acknowledgements

This research was supported by the National Science Foundation Grants AGS-1016095 and AGS-1118429. The ERA-Interim data were downloaded from the Research Data Archive at the National Center for Atmospheric Research, Computational and Information Systems Laboratory (NCAR CISL). The project was also made possible by adviser Zhuo Wang, who oversaw progress through the duration of the study. The doctoral committee was instrumental in guidance as well, which was filled by Bob Rauber, Stephen Nesbitt, and Timothy Dunkerton. Graduate students Gan Zhang, Cody Fritz, and Wei-Wei Li provided assistance in data analysis.

Table of Contents

Chapter 1: Introduction

Tropical cyclone formation is the least understood phase of the tropical cyclone lifecycle and thus is one of the most challenging issues in tropical meteorology. Although the large-scale necessary conditions for genesis were identified more than four decades ago (Gray 1968), the formation of the tropical cyclone vortex within a synoptic scale wave has been regarded, until recently, as a mystery.

Tropical easterly waves (TEWs) play an important role in tropical cyclogenesis over the Atlantic (e.g., Landsea 1993). Most, but not all of these synoptic-scale disturbances are triggered by finite-amplitude, transient heating in the African easterly jet (AEJ) entrance region and develop via a combined barotropic-baroclinic growth mechanism (e.g., Thorncroft et al. 2008), which are also called African easterly waves (AEWs). They are characterized by a typical period of 2-5 days and a wavelength of 2000-4000 km (Carlson 1969; Reed et al. 1988a), and propagate westward along the easterly jet over West Africa and the East Atlantic. The waves often get enhanced near the coast by convection, and the baroclinic characteristics of AEWs erode as the waves propagate over the Atlantic. With favorable large-scale conditions, some waves, about 20%, intensify into tropical cyclones (Frank 1970).

Some previous studies have suggested that the development of a tropical cyclone is related to the structure and/or intensity of the precursor wave disturbance (Ross and Krishnamurti 2007; Hopsch et al. 2010; Peng and Fu 2010; Fu and Peng 2010; Wang et al. 2010). In particular, Kiladis showed that the distribution of active, deep convection is associated with adiabatic dynamical forcing implied by the advection of perturbation vorticity by the mean thermal wind in the zonal direction (Kiladis et al. 2006). Deep

convection plays an important role in spinning up vorticity near the surface through the aggregation of vortical hot towers (VHTs) and concentration of the ambient vorticity (Hendricks et al. 2004; Montgomery et al. 2006). TC genesis is thus a multi-scale process which involves the meso-β scale convective organization of a TC vortex within a synoptic-scale wave (Dunkerton et al. 2009). To properly address this issue, we need to investigate the spinup of the tropical cyclone proto-vortex, the organization of moist convection, and the resulting warm core formation in the days approaching genesis from the dynamic and thermodynamic perspective.

1.1 The marsupial paradigm

The recently proposed marsupial paradigm for tropical cyclone formation within tropical easterly waves provides a framework from which to examine the multi-scale interaction involved in tropical cyclone formation (Dunkerton et al. 2009). Using high-resolution model simulations, Wang et al. (2010a, b) and Montgomery et al. (2010) showed that the recirculation region within the wave critical layer, or the so-called wave pouch, acts as the "guiding hand" for the aggregation of convective-scale vorticity anomalies. Although the genesis time and the intensity of the proto-vortex depend on mesoscale processes and have limited predictability, the genesis location is largely controlled by the parent wave's critical layer (Wang et al. 2010b). Since global models can forecast synoptic-scale disturbances with reasonable skill, the track of the preferred genesis location, i.e., the wave pouch center, can be predicted using global model operational data (Wang et al. 2009). The forecasts of pouch tracks and evolution based on the marsupial paradigm have been used in some recent field experiments, including TCS-08 (Elsberry and Harr 2008), PREDICT (Montgomery et al. 2012) and GRIP (Braun et al. 2013) to provide useful

guidance on flight planning. Using the wave pouch tracks, the dynamic and thermodynamic properties and evolution of TEWs will be investigated during tropical cyclone formation in this study.

1.2 Interaction between two groups of African easterly waves and the formation of Cape Verde storms

The popular nomenclature of "Cape Verde" storms refers to tropical cyclones that form over the East Atlantic, near the Cape Verde Islands. Since these storms form over the eastern portion of the ocean basin, they generally have a longer propagation time period over the warm ocean before recurving northeastward or making landfall, and thus are more likely to develop into major hurricanes. Cape Verde storms often form shortly after an AEW moves from land to ocean. The properties of AEWs and the regional climate conditions over West Africa presumably have significant impacts on the formation of such storms.

Previous studies show that there are two wave tracks over West Africa: one to the north and the other to the south of the AEJ (Pytharoulis and Thorncroft 1999; Ross and Krishnamurti 2007). The two groups of disturbances have different vertical structures and thermodynamic properties. The waves south of the jet peak at the jet level (600-700 hPa) with a cold core structure in the lower troposphere, and are often associated with squall lines and precipitation. The northern disturbances are primarily confined to 850 hPa and below. Located north of the jet, they are much drier and are often associated with dust outbreaks (e.g., Karyampudi et al. 1997). While the southern waves propagate along the zone of strong potential vorticity gradient, the northern waves follow the positive meridional gradient of potential temperature (Pytharoulis and Thorncroft 1999; Thorncroft and Hodges 2001).

Most previous studies focus on the waves propagating south of the jet axis because of the associated convective activity and the potential for tropical cyclone development. While some of the northern disturbances decay off the coast or move northwestward, most of them move southwestward, some of which interact with the waves in the southern track (Reed et al. 1988b). Pytharoulis and Thorncroft (1999) speculated that such an interaction may enhance the probability of tropical cyclogenesis as the northern waves have strong vorticity features near the surface. On the other hand, they pointed out that the dry air associated with the northern waves may promote convective downdrafts and act as a negative factor for genesis. Furthermore, Ross and Krishnamurti (2007) examined the AEW activity and its relationship to Atlantic tropical cyclogenesis in 2001, and suggested that the two wave regimes can interact with each other and both are instrumental in tropical cyclogenesis. In contrast, Zawislak and Zipser (2010) suggest that the northern 850 hPa disturbances generally do not interact with the moist southern disturbances. Chen et al. (2008) suggested that the northern waves led to a large number of tropical cyclones. Although the controversy can be partly attributed to the different methodologies for wave tracking or identification of a northern wave, it reflects our limited understanding of the interaction between the two groups of waves and highlights the need for further study.

The wave merger scenario between the two tracks is intriguing due to its potential to impact the low level vorticity evolution on the mesoscale over the Atlantic. Highlighting the importance of low-level vorticity, McBride and Zehr (1980) found that the low-level vorticity in the vicinity of a developing system is stronger than and twice as large as in a non-developing system. Wang et al. (2010) suggested that a deep wave pouch structure extending from 600 hPa to the boundary layer is a necessary condition for tropical cyclone

formation. Since the vorticity disturbances in the northern track exist in the 1000-850 hPa layer primarily, it follows that an offshore merger with the southern disturbances could add the necessary low-level vorticity for development to occur or help to create a deep wave pouch. In many cases the northern and southern waves both have closed pre-merger pouch circulations, which enable simultaneous tracking of multiple circulations impacting the complex structure of the TC proto-vortex over Africa for several days prior to the merger. This is a distinct advantage of the pouch tracking from the marsupial paradigm, which provides the opportunity to conduct diagnoses on important dynamics and thermodynamics such as the circulation characteristics, moisture distribution, and vertical wind shear across multiple scales relative to the pouch center. One of the objectives of this study is to examine the dynamic and thermodynamic evolution of the wave pouches during the merger of a northern wave with a southern wave and the impacts of the merger on the subsequent storm development.

1.3 Impacts of dry air on tropical cyclone formation

One of the detrimental factors for tropical cyclone formation is dry air. The presence of dry air at the midtroposphere in the tropics is well known to affect deep convection associated with tropical cyclone formation (Yoneyama and Fujitani 1995; Mapes and Zuidema 1996; Lucas et al. 1996). Dry air entrainment reduces cloud buoyancy and hinders the development of deep convection and tropical cyclone formation. The marsupial paradigm suggests that an area of recirculation around the intersection between the critical latitude and wave trough provides the tropical cyclone embryo protection from the surrounding environment to some degree. This makes the wave pouch center a favorable location for tropical cyclogenesis, and the existence of a wave pouch was found

to be a necessary condition for developing systems (Wang et al. 2009; Wang et al. 2010). However, a closed circulation often is absent in the upper troposphere at the early stage. This makes the upper troposphere a region of vulnerability to the influence of dry air (Fritz and Wang 2013), particularly in the early formation stages. Other recent findings have shown that midtropospheric moistening is a critical process for tropical cyclone formation near the pouch center (Wang 2014), and that intensifying systems have higher environmental relative humidity than weakening storms (Wu et al. 2012). Given the context that tropical cyclone formation is associated with moisture preconditioning, understanding the occurrence of synoptic scale dry air intrusion and its interannual variability helps us better understand and predict the variability of tropical cyclone activity.

Dry air over the Atlantic has at least two possible sources: the Saharan Air Layer (SAL) and midlatitude intrusion. Dunion and Velden (2004) highlighted the detrimental impacts of the SAL on tropical cyclone intensification. Braun (2010) examined these claims about the SAL by analyzing storms based on their occurrence in association with African Easterly Waves (AEWs) and along SAL outbreaks. Braun (2010) used layer-averaged RH to define dry air events, and showed that seasonal variations in the 600-700 hPa layer RH are independent of SAL outbreaks. Instead, the dry air was found in association with large-scale troughs on either side of a Saharan midlevel high pressure system. The study did find that the SAL inhibits deep convection within the SAL, restricting convection to the south, but it is not known whether this actually inhibits storm development in any way to the south of the African Easterly Jet (AEJ). Furthermore, Casey et al. (2009) showed that anomalously dry middle and upper tropospheric air originates in the subtropics. Zhang and Pennington (2004) showed that dry air events can be independent

of African dust outbreaks. Other studies have confirmed that dry air often originates in association with anticyclonic flow in the subtropics and is ultimately induced by midlatitude processes before being advected southward through meridional flow around anticyclones (Yoneyama and Parsons 1999; Huang et al. 2010). The impacts of upper tropospheric dry air on tropical cyclones have been suggested by some studies (Braun 2010; Hopsch et al. 2010; Fritz and Wang 2013). The interannual variations of the dry air frequency in the tropical North Atlantic, however, remain unclear. A documentation of the interannual variability of dry air intrusions and the linkage to large-scale climate factors could be useful in forecasting on the seasonal and synoptic time scales.

This study consists of three parts. In the first part (chapter 2), the dynamic and thermodynamic evolution of tropical easterly waves at the pre-genesis stage is examined via composite analysis based on the tracking of more than 150 named storms over the Atlantic. In the second part (chapter 3), we focus on the formation of the Cape Verde storms and examine the impacts of the merger between a northern wave and a southern wave. In the last part (chapter 4), the interannual variability and impacts of the middle and upper tropospheric dry air occurrence are examined. A brief summary with some discussions is presented in the last chapter.

Chapter 2: Characteristics of TEW Pouches during Tropical Cyclone Formation

2.1 Background

The thermodynamic structure of the wave pouch and its impacts on moist convection and tropical cyclone formation were examined by Wang (2012) through the analysis of a numerical model simulation and dropsonde data from the PREDICT field experiment. It was found that the meso-β area near the pouch center (or the inner pouch region) is characterized by high saturation fraction and a short incubation time scale, which are believed favorable for deep convection and genesis. The analysis of dropsonde data showed that the mid-level equivalent potential temperature (θ_e) increases significantly near the pouch center one to two days prior to genesis but changes little away from the pouch center, which may indicate convective organization and the impending TC genesis near the pouch center. The difference between the inner pouch and outer pouch region was also observed by Davis and Ahijevych (2013).

Wang (2012) was based on the numerical simulation of a single storm and the dropsonde data analysis of limited cases. *The objective of this chapter is to examine the dynamic and thermodynamic evolution of wave pouches, especially the difference between the inner pouch region and the meso-α scale wave pouch, with a much larger sample size (164 named tropical cyclones) using the ERA-Interim data and CMORPH precipitation.*

2.2 Data and methods

The ERA-Interim reanalysis (Simmons et al. 2007) is the latest ECMWF global atmospheric reanalysis. It utilizes 4DVAR and provides a more realistic representation of the atmosphere in both space and time than earlier reanalysis datasets. The spatial

resolution of the data is about 0.7 degrees, which is marginal to study meso-β scale structures, but as shown later, the data capture the statistically significant differences between the inner pouch region (meso-β) and the pouch scale (meso-α). Three-hourly precipitation from the CMORPH (CPC MORPHing technique) dataset (Joyce et al. 2004), with spatial resolution of 0.25°, was used as a proxy for convection. The precipitation estimates were derived from low-orbiting satellite microwave observations exclusively, and motion vectors derived from geostationary satellite IR data were used to propagate precipitation features. For the ERA-Interim data, we used a ~1.4° square box (3X3 grid points) to represent the inner pouch region, and a ~4.2° square box (7X7 grid points) to represent the pouch scale; for the CMORPH data, we used a 1.5° square box (7X7 grid points) to represent the inner pouch region, and a 4° square box (17X17 grid points) to represent the pouch scale. All the boxes are centered at and moving with the propagating pouch centers at 700 hPa.

The TC genesis time and locations were obtained from the National Hurricane Center (NHC) Best Track data. The wave pouch center was determined by the intersection of the wave trough axis and the wave critical latitude. The phase speeds of precursor waves were derived from the linear regression of the band-pass filtered (Doblas-Reyes and De´que´ 1998) 700 hPa meridional wind, following Dunkerton et al. (2009). The wave pouch was then tracked at 700, 850 and 925 hPa backward in time from genesis to Day -10 (ten days prior to genesis) as long as a well-defined wave pouch was present. We focus on the named tropical cyclones over the Atlantic in July-October 1989-2010. There were 255 named storms during this time period. After excluding 41 storms without well-defined zonal propagating signals in the Hovmöller diagrams, 1 subtropical cyclone, 22 tropical

storms without a wave pouch at 700 hPa at genesis[1], and 27 waves with meridional propagation speed larger than 3.0 m s^{-1}, we have 164 storms left. The statistical analyses in the following section are based on the 164 storms.

2.3 Results

The pouch tracks at 700, 850 and 925 hPa are shown in Fig. 2.1a. Also shown is the axis of the 700 hPa easterly jet. Over the Atlantic Main Development Region (MDR; 80°-20°W, 10°-20°N), most of the pouch tracks are located south of the long-term mean jet axis. Among the 164 storms, 41 pouches at 700 hPa can be tracked back east of 10°W, some of them extending as far as 10°E. In contrast, only ten (two) pouch tracks at 850 (925) hPa are present east of 10°W, suggesting that most wave pouches over West Africa have a shallow structure confined to ~700 hPa. This can be attributed to the strong vertical shear in the lower troposphere over West Africa. A significant increase in the 850 and 925 hPa pouch track density near the coast suggests that wave pouches tend to develop a deep structure after moving over to the ocean, probably due to the coastal convection and a decrease in the vertical wind shear. A secondary wave track is discernible over West Africa north of the jet axis[2] (e.g., Carlson 1969; Burpee 1974; Nitta and Takayabu 1985; Pytharoulis and Thorncroft 1999). Wave pouches are confined below 850 hPa along this northern track, and they move southwestward off the coast merging with the southern wave track (e.g., Reed et al. 1988a; Thorncroft and Hodges 2001). Pouch tracks are also present north of the jet over the West Atlantic and the Gulf of Mexico. These tracks are generally

[1] Some of the 22 storms have a wave pouch present at 850 or 925 hPa at genesis. They are excluded because the wave evolution is examined following the 700 hPa pouch track.
[2] Note that Fig. 1.1a only shows northern waves that have a closed circulation in the wave's co-moving frame of reference. Not all northern waves have a pouch.

shorter than those in the MDR region. Some of the pouches may be associated with wave disturbances forming over the Atlantic or associated with midlatitude frontal systems.

Tropical cyclogenesis locations are shown in Fig. 2.1b. Over West Africa, the East and Central Atlantic (east of 60°W), most of the wave pouches (~80%) formed at 700 hPa first, while about 68% of tropical cyclones over the West Atlantic (west of 60°W) had a wave pouch forming at 925 or 850 hPa first. This is related to the zonal variations of the mean flow. Over West Africa and the East Atlantic, the mean flow is characterized by a well-defined, meridionally confined jet peaking at 600-700 hPa. The jet weakens westward and gradually transitions into a broad region of trade wind easterlies peaking at 850-900 hPa over the West Atlantic. Also shown in Fig. 2.1b is the long-term mean convergence at 850 hPa during July-October. Nearly all the tropical cyclones developed in a region of low-level convergence.

The distribution of wave pouch lifetime is shown in Fig. 2.2a. Among the 164 named storms, 97%, 90%, 82% and 79% of them have a wave pouch form by 12 hours prior to genesis at 700 hPa, 850 hPa, 925 hPa, and all of the three levels, respectively. 32% of the storms have a pouch form at 700 hPa more than five days prior to genesis. Wang et al. (2012) suggested that a deep wave pouch extending from ~600 hPa down to the boundary layer is a highly favorable condition for genesis. Other factors that need to be considered for genesis include SST, vertical shear, etc. (e.g., Gray 1968).

The vertical displacement of the wave pouches with respect to 700 hPa, which is defined as the distance between the pouch centers at two levels, is examined in Fig. 2.2b. On average, there is a one to two degrees displacement within three days prior to genesis. The displacement has a general tendency of decreasing approaching the genesis time,

which is consistent with the study by Dunkerton et al. (2009) using a smaller sample size. A vertically aligned wave pouch is believed to be a favorable condition for genesis (Wang et al. 2012; Raymond and López Carrillo 2011; Davis and Ahijevych 2012).

To examine the dynamic evolution of the wave pouch at different spatial scales, the 925 and 700 hPa relative vorticity and the Okubo-Weiss parameter[3] (OW) averaged over the inner pouch region and the meso-α pouch scale are shown in Figs. 2.3. The difference between the inner pouch and the pouch-scale averages implies a difference between the inner and outer pouch regions. An evident feature in Figs. 2.3a and 2.3b is that the mean vorticity and OW at the inner pouch are much stronger than those averaged over the pouch scale, suggesting that the inner pouch region is characterized by stronger rotation and weaker deformation compared to the outer pouch region. The averages over the inner pouch region and over the pouch scale both show stronger vorticity and OW at 700 hPa than 925 hPa at the early stage, which is consistent with the typical vertical structure of an African easterly wave (e.g., Reed et al. 1988b). However, due to a larger intensification rate at 925 hPa, the 925 hPa vorticity (and OW) exceeds that at 700 hPa 18 hours prior to genesis in the inner pouch region, suggesting the formation of a warm-core structure at the meso-β scale. At the pouch scale the relative vorticity at 925 hPa becomes close to but does not exceed that at 700 hPa, and a well-defined warm-core structure is absent even at genesis. The different vorticity evolutions at different spatial scales are consistent with the numerical model simulation in Wang (2012). Wang (2012) showed that vorticity evolves

[3] The OW parameter is a measure of the "shape-preserving" component of a vortical flow (Rozoff et al. 2006; Dunkerton *et* al. 2009) and is defined by OW = $\zeta^2 - S_1^2 - S_1^2$, where ζ is relative vorticity and $(S_1^2 + S_2^2)$ represents the strain rate. Positive values of OW indicate that the flow is rotation-dominant, and negative values of OW suggest that the flow is susceptible to rapid filamentation.

differently at different spatial scales: the spin-up of the meso-β scale low-level circulation near the pouch center precedes the spin-up of the mid-level vortex, while at the meso-α pouch scale vorticity increases in the middle troposphere first. Wang (2012) attributed the different vorticity evolution to the different thermodynamic conditions in the inner and outer pouch regions and the resultant convective distribution.

Figure 2.3c shows the 975 hPa convergence averaged at the two different scales. At the early stage the two averages have large fluctuations and are close to each other. From t=-30 h onward, the convergence averaged over the inner pouch region exceeds that averaged at the pouch scale, indicating that convection has begun to organize near the pouch center. The time series of precipitation rate conveys the same message. Also notable in Fig. 2.3a is a larger intensification rate of relative vorticity within 24 hours prior to genesis compared to the early stage. The rapid intensification in vorticity coincides with the significant increase in the low-level convergence and precipitation within ~24 hours prior to genesis, and is consistent with an abrupt transition to strong deep convection shortly before genesis suggested by Wang (2013).

The thermodynamic condition of the wave pouch is examined in Fig. 2.4. The differences in specific humidity (SH), air temperature (T) and θ_e between the inner pouch region and the pouch scale were calculated. The significance of the differences was examined in two student's-t tests. In the first test, the inner pouch average and the pouch-scale average of a storm are treated as a paired observation, and a one-sample one-sided t test is carried out with the null hypothesis that the difference between the inner pouch and the pouch-scale averages is zero. In the second test, the inner pouch averages and the pouch-scale averages are treated as independent samples, and a two-sample one-sided t test

is carried out with the null hypothesis that the inner pouch averages and the pouch-scale averages have the same sample means. The second test is stricter (or more sensitive) than the first test (Wilks 2006, Chapter 5.2).

Figure 2.4a shows that the inner pouch has larger specific humidity than the pouch-scale average. The magnitude of the difference is very small (<=0.2 g kg $^{-1}$), but it exceeds the 99% confidence level for paired samples at most vertical levels from t=-72 h to genesis, and exceeds the 99% (95%) confidence level for independent samples between 550-800 hPa within 18 (24) hours before genesis. The higher water vapor content in the inner pouch region is consistent with the findings by Wang (2012) in a high-resolution numerical model simulation and dropsonde data analysis. Wang (2012) suggested that the high moisture content in the inner pouch region is related to the dynamic and kinematic structure of the wave pouch and contributes to convective organization near the pouch center. Figure 2.4a is also consistent with Nolan (2007), who emphasized the importance of column moistening for tropical cyclogenesis.

Figure 2.4b shows that the inner pouch is relatively warmer than the pouch scale above 700 hPa and colder below. The difference exceeds the 99% confidence level for paired samples most of the time but does not exceed the 95% confidence level for independent samples. Significant cold anomalies in the lower troposphere become more confined near the surface within the 24 hours prior to genesis. Despite the small magnitude (less than 0.1 K at most levels), the temperature difference is consistent with the transition of the circulation from a cold-core structure to a warm-core structure near the pouch center (Fig. 2.3a). The temperature difference also indicates enhanced static stability in the inner pouch region, which was also reported by Davis and Ahijevych (2013) in dropsonde data

analysis. Raymond et al. (2011) suggested that a mid-level vortex with the associated enhanced static stability helps to create a more conducive environment for tropical cyclone formation by making the vertical mass flux profile of deep convection more bottom-heavy. Although Fig. 2.4b indicates enhanced static stability at the inner pouch region, it is worth pointing out that the temperature difference is present more than 3 days prior to genesis and does not show progressive change as the moisture field does. Besides being consistent with the vertical structure of the circulation, the significance of the temperature field and enhanced static stability to convection and genesis can not be determined by the analysis here. Instead, the steady increase in mid-level moisture suggests the importance of mid-level moistening.

Figure 2.4c shows that the inner pouch region has higher θ_e than the pouch scale average above the boundary layer. The difference maximizes around 700 hPa and exceeds the 99% (95%) confidence level for independent samples within 18 (24) hours prior to genesis. Comparison between Figs. 2.4a and 2.4b suggests that the difference in θ_e mainly results from the humidity difference, which is consistent with Wang (2012). Given the spatial resolution of the ERA-Interim data, it is not a surprise that the magnitude of the difference is much smaller than that derived from dropsonde data.

2.4 Summary

The evolution of wave pouches prior to genesis was examined for 164 named tropical cyclones that originated from zonally propagating tropical easterly waves over the Atlantic during 1989-2010. It was found that most (~80%) wave pouches east of 60°W form at 700 hPa first. A wave pouch over West Africa is often confined to around 700 hPa, and tends to extend to 850 or 925 hPa off the coast of West Africa. Over the West Atlantic

(east of 60°W), a larger fraction (68%) of wave pouches develop at 850 or 925 hPa first. A wave pouch becomes more vertically aligned approaching genesis.

The evolution of vorticity and OW shows that the circulation at 925 hPa intensifies faster than that at 600 hPa. A warm-core structure develops at the meso-β scale near the pouch center prior to genesis, but a well-defined warm core structure is absent at the meso-α pouch scale. The comparison of precipitation and the low-level convergence evolution between the inner pouch region and the meso-α pouch scale suggests that convection becomes organized or concentrated near the pouch center about one day prior to genesis, which coincides with a rapid intensification in vorticity in the inner pouch region. The ERA-Interim composites also show significant moistening in the inner pouch region, especially at the middle troposphere within one day prior to genesis.

2.5 Figures

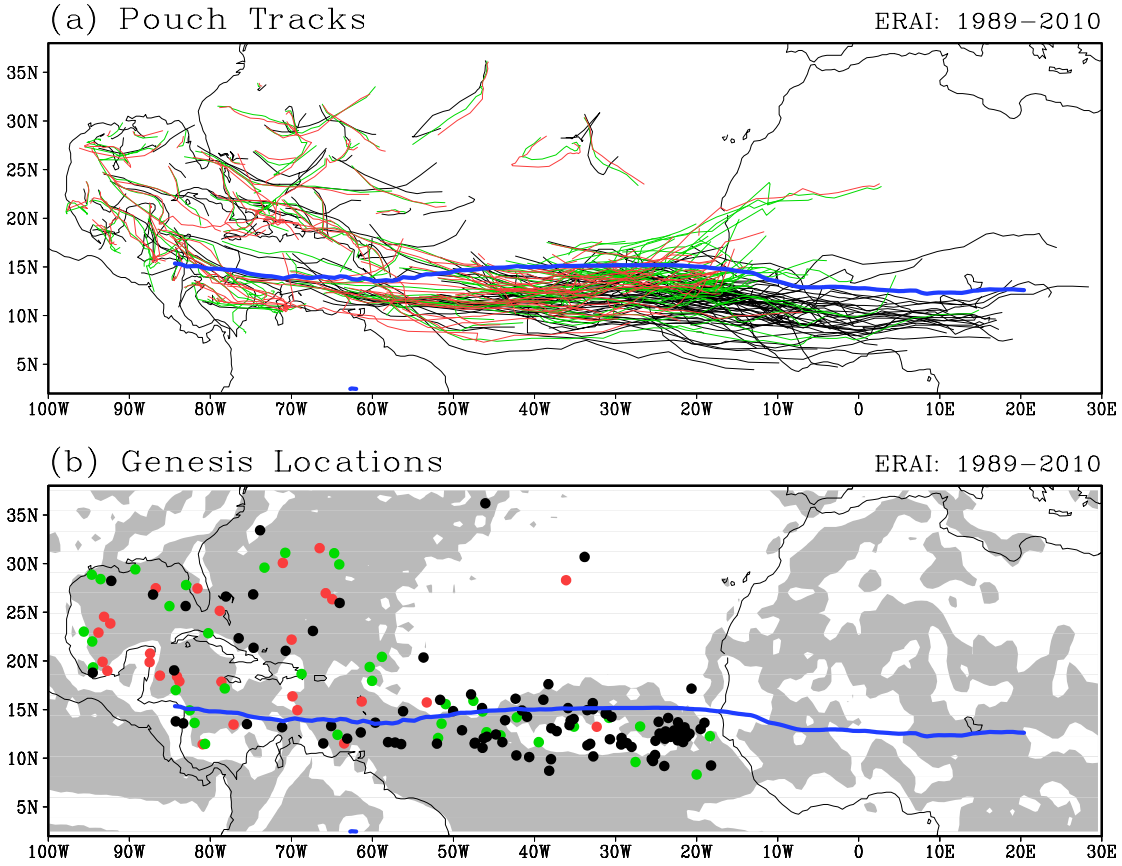

Figure 2.1 (a) Wave pouch tracks at 700 (black), 850 (green) and 925 (red) hPa; (b) the TC genesis locations. Black, green and red colors in (b) represent TCs that have a wave pouch first forming at 700, 850 and 925 hPa, respectively. Shading in (b) indicates regions of mean convergence at 850 hPa from the long-term mean during 1989-2010 July-Oct. The thick blue curve represents the axis of the 700 hPa easterly jet from the long-term mean during 1989-2010 July-Oct.

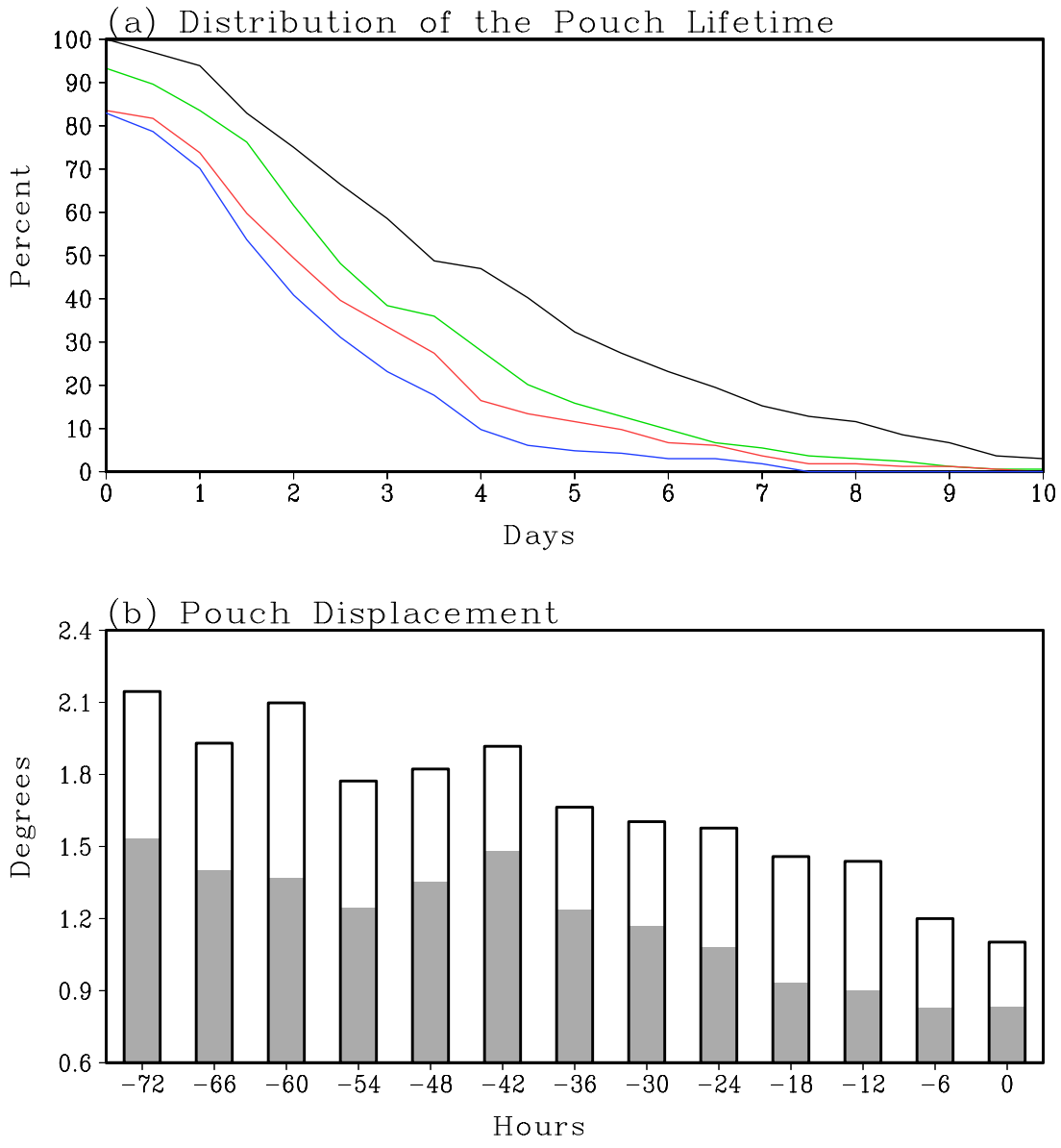

Figure 2.2 (a) The percentages of waves with the pouch lifetime equal to or longer than the indicated time (the abscissa; units: days) at 700 hPa (black), 850 hPa (green), 925 hPa (red) and all of the three levels (blue); t=0 day indicates the percentages of waves having a pouch at genesis. (b) The mean displacement (units: degrees) of the 850 (gray bars) and 925 (open bars) hPa wave pouch centers with respect to the 700 hPa pouch centers.

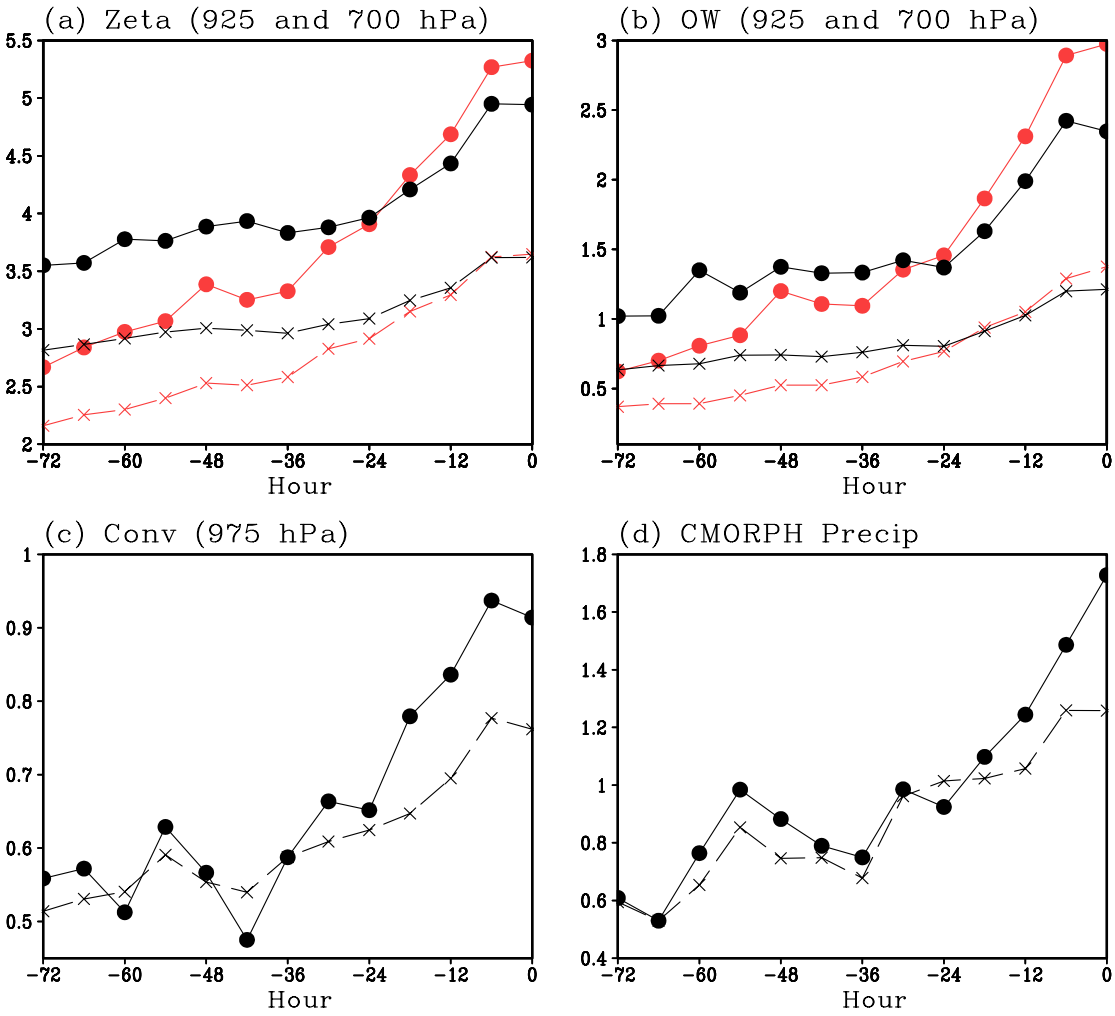

Figure 2.3 Areal averages of (a) 925 hPa (red curves) and 700 hPa (black curves) vorticity (units: 10^{-5} s^{-1}), (b) 925 hPa (red curves) and 700 hPa (black curves) OW (units: 10^{-9} s^{-2}), and (c) 975 hPa convergence (units: 10^{-5} s^{-1}) derived from ERA-Interim for 1989-2010; (d) precipitation rate (mm $hour^{-1}$) derived from the CMORPH dataset for 2003-2010. Multiplication signs represent averages over the pouch scale, and closed circles represent averages over the inner pouch area.

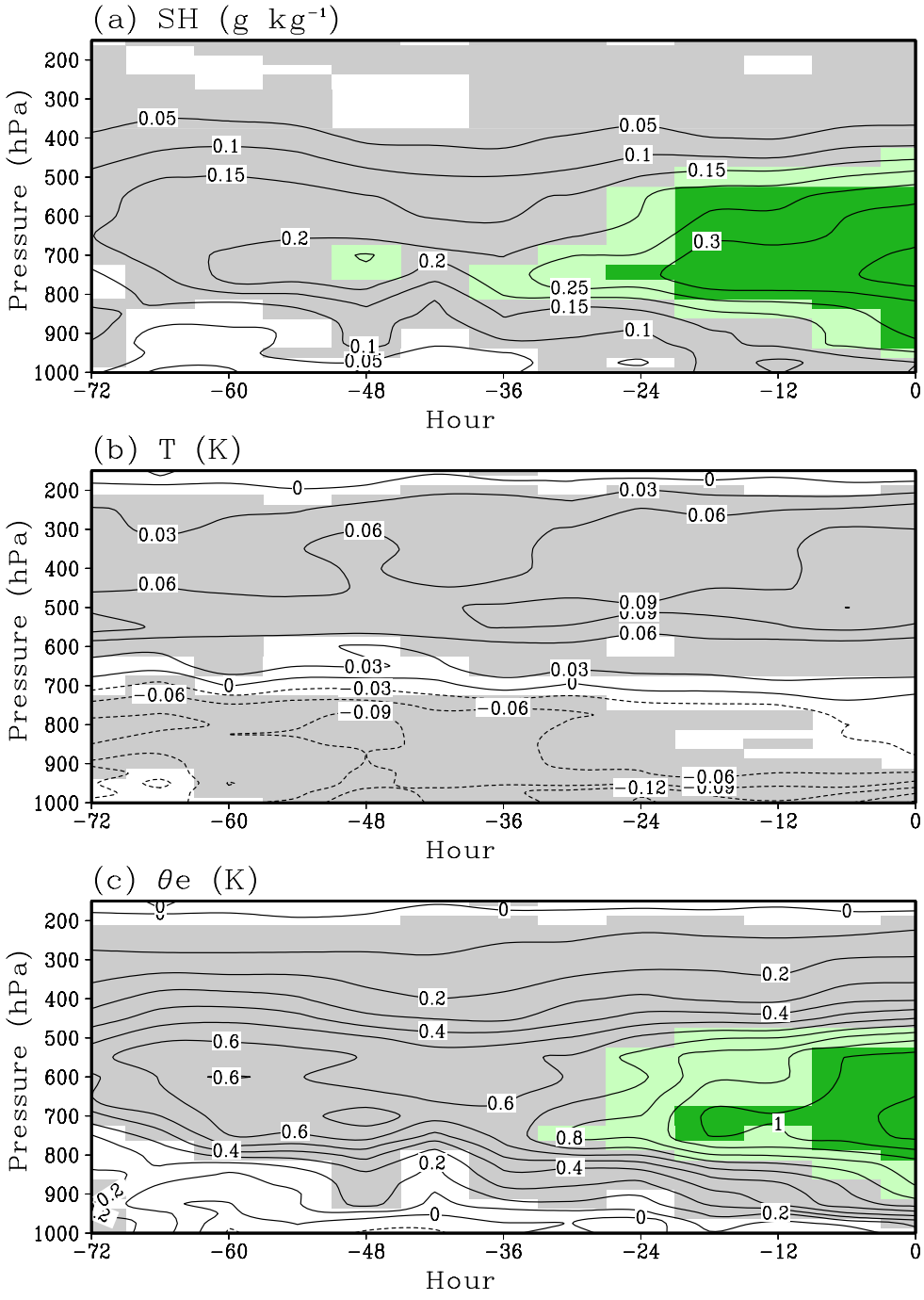

Figure 2.4 Differences of (a) specific humidity (units: g kg^{-1}), (b) air temperature (units: K), and (c) equivalent temperature (units: K) between the inner pouch averages (~1.4°) and the pouch scale averages (~4.2°) from 72 hours prior to genesis to the genesis time. Gray shading highlights differences exceeding the 99% confidence level for paired samples, and light and dark green shadings highlight differences exceeding the 95% and 99% confidence levels for independent samples, respectively.

Chapter 3: Impacts of East Atlantic TEW Mergers and Middle to Upper Tropospheric Dry Air on Tropical Cyclone Formation

3.1 Background

In this chapter, we will examine the merger of the southern waves with the northern disturbances and the dynamic and thermodynamic evolution of their structures during the merger. In particular, we will address the following questions:

- How often do the mergers occur, and how do they lead to development/non-development?
- What synoptic/mean flow conditions cause the mergers to occur?
- How do mergers differ from non-mergers?

We will employ the framework of the marsupial paradigm (Dunkerton et al. 2009). The marsupial paradigm proposes that the approximately closed Lagrangian circulation within the wave critical layer, or the wave pouch, provides a local favorable environment for vorticity aggregation and convective organization that lead to tropical cyclone formation (Wang et al. 2010a; Wang 2012; Wang 2014), and that the center of the wave pouch is the preferred location for genesis. Wang et al. (2012) suggested that a deep pouch extending from 600-700 hPa to near the surface is a necessary condition for cyclogenesis. They also showed that the merger between an AEW and a disturbance in the Inter-Tropical Convergence Zone (ITCZ) led to a stronger and deeper wave pouch, which later developed into Tropical Cyclone Erika (2009). Similar to the northern waves, the ITCZ disturbance had a shallow structure and was initially confined to 850 hPa and below. Here we will test the hypothesis that *the merger of a northern wave and a southern wave helps to create a stronger and deeper wave pouch that is more conducive to tropical cyclone formation*.

3.2 Data and Methodology

The 6 hourly ERA-Interim reanalysis (Simmons et al. 2007) were used to track easterly waves and examine their dynamic and thermodynamic evolution. The ERA-Interim data have the horizontal resolution of ~0.7 degrees and can resolve the mesoscale structure of a wave pouch to some extent as shown in chapter 2. The phase speeds of precursor waves were derived from the linear regression of the band-pass filtered (Doblas-Reyes and De´que´ 1998) 700 hPa meridional winds (Dunkerton et al. 2009; Wang and Hankes 2014). The wave pouch center, or the preferred location for genesis, is determined by the intersection of the wave trough axis and the wave critical latitude. The wave pouches were tracked at 700, 850 and 925 hPa backward in time from genesis to up to 10 days prior to genesis as long as a well-defined wave pouch was present.

Moderate Resolution Imaging Spectroradiometer (MODIS) Level 3 (Hubanks et al. 2008) Aerosol Optical Depth (AOD) dataset was used to examine the aerosol distribution associated with dry air. The dataset provides daily AOD estimates on a 1° × 1° global grid based on observations of Terra/Aqua satellite platforms. The data were acquired from NASA Goddard Space Flight Center data server (ftp://ladsweb.nascom.nasa.gov/allData/51/), where retrievals from Terra and Aqua are stored separately. The Terra subset is available from 2000 to the present and the Aqua subset is available since 2002. We chose the time period of 2002-2012, when both subsets are available. Additionally, infrared (IR) data from the Cooperative Institute for Meteorological Satellite Studies (CIMSS) Tropical Cyclone Archive (http://tropic.ssec.wisc.edu/archive/) are used to examine the convective evolution.

A northern wave disturbance is identified as a westward propagating low-level (925-850 hPa) vorticity feature with a maximum equal to or exceeding 2×10^{-5} s^{-1} originating north of the easterly jet axis. The criterion of a propagating feature is to exclude stationary vorticity features in association with the monsoon trough or the Saharan heat low, which are common over West Africa. Northern disturbances are typically, but not always, accompanied by a closed pouch circulation in the co-moving frame of reference. A southern wave is tracked at 700 hPa and propagates south of the jet axis over Africa. Note that although they are referred to as two groups of waves, it does not imply that the northern waves and the southern waves are independent of each other. Both may be part of the same African easterly wave of a complex structure (Pytharoulis and Thorncroft 1999).

A merger event is defined as the sequence in which a northern wave moves southwestward, often near the coast, and becomes horizontally overlapped (or vertically aligned) with a wave pouch south of the AEJ axis. The merger time is defined as the time at which the pouch centers between the disturbances are 3 degrees or less apart in horizontal distance for cases that a closed pouch exists north of the jet axis. In cases that the northern wave does not have a closed circulation, the merger time is defined as the time at which the northern vorticity patch (at least 2×10^{-5} s^{-1}) and the southern wave pouch at 700 hPa are 3 degrees or less apart in horizontal distance. The implementation of these criteria is illustrated for Isabel (2003) in the next section.

It is worth pointing out that not every northern wave merges with a southern wave. For example, the precursor wave of Danielle (2010) was accompanied by a northern wave disturbance at 850 hPa, but the northern disturbance never merged with the southern wave. Merger may also occur after genesis. For example, Igor (2010) absorbed a disturbance to

its east that originated north of the jet over West Africa, and the merger seemed to help intensify Igor. Such cases are excluded in our analyses because we are interested in the impacts of merger on the subsequent storm formation prior to genesis.

Three groups of AEWs are examined: i) merger developers: AEWs that merge with a northern wave and develop into a tropical cyclone over the East Atlantic; ii) non-merger developers: developing AEWs that are not involved with merger; and iii) merger non-developers: AEWs that merge with a northern wave but do not develop into a tropical cyclone over the East Atlantic. For the first two groups, we focus on the formation of named storms during 1989-2012 over the East Atlantic (east of 40°W), for which the merger of two disturbances is expected to have immediate impacts on the storm formation. The merger non-developers were selected from the non-developers archived in the marsupial tracking products (Wang et al. 2009) at the Naval Postgraduate School (http://met.nps.edu/~mtmontgo/marsupial.html) from 2008-2012. Merger non-developers were identified using the same criteria described above. Different from non-developers examined in some previous studies (e.g., Peng et al. 2011; Fu et al. 2011; Kerns 2009), the non-developing waves examined in this study all have a well-defined wave pouch sometime during their lifetime. The merger developers are compared with the non-merger developers to examine the impacts of merger on the subsequent storm development, and the merger non-developers are examined to investigate the key processes or environmental factors for tropical cyclone formation.

As shown in Figure 3.1, the number of merger developers per year is much lower than the number of merger non-developers or the number of non-merger developers per year. It suggests that only a small fraction of the East Atlantic tropical cyclones (~31%)

are involved with a merger and that only a small fraction of mergers (20%) intensify into tropical cyclones. Although merger occurs from July to September with the peak frequency in September, merger developers only occur in August and September (Fig. 3.2) in the time period examined (1989-2012). Merger and non-merger developers have similar genesis locations under the longitude criterion (east of 40°W) used for case selection. A noticeable difference between the merger non-developers and developers is the merger location. On average, the merger location for non-developers is about 3 degrees north and 1 degree west of the merger location for developers (Figure 3.1). The latitudinal displacement is particularly significant, as it is greater than one standard deviation. The differences between merger developers and non-developers are examined in detail in a later section, and student's t-tests were performed to test the significance of the composite difference.

The analyses in the following sections are conducted in the wave's co-moving frame of reference and centered on the pouch center to examine the quasi-Lagrangian evolution if not specified otherwise. The mean phase speed between 700 hPa and 850 hPa for each storm was used to translate the frame of reference. The mean phase speed is -7.4 m s^{-1} for non-merger developers, -7.8 m s^{-1} for merger developers, and -8.0 m s^{-1} for merger non-developers.

3.3 A Typical Developing Merger Case: Isabel (2003)

Streamlines and vorticity

Isabel in 2003 was chosen to highlight the key features of a typical merger event. According to the National Hurricane Center (NHC) report (Beven and Cobb 2004, http://www.nhc.noaa.gov/2003isabel.shtml), Isabel developed from a tropical wave that departed the west coast of Africa on 1 September. The wave gradually became better

organized as it propagated westward, and a tropical depression formed at (28.6°W, 13.8°N) at 00Z on 6 September. The zonal phase speed of the wave averaged over the 700- and 850-hPa levels is -4.9 m s^{-1}. A pouch in the southern disturbance can be tracked back 114 hours prior to genesis at 700 hPa. Figure 3.3 shows the evolution of relative vorticity from 06Z on 31-August to 06Z on 5-September, at 24 hour increments. Two levels are chosen: 700 hPa, which captures the southern wave track, and 850 hPa, which is around the peak altitude of the northern disturbance (e.g., Reed et al. 1988b; Pytharoulis and Thorncroft 1999). Streamlines are shown in the co-moving frame of reference. The pre-Isabel wave is associated with a clear disturbance in both the southern and northern wave tracks, each with a closed pouch circulation. At the beginning of the time sequence (06Z 31-August), the 850 hPa pouch is visible as a closed circulation centered at (2°E, 22°N) and embedded within a northeast-southwest oriented trough north of the AEJ axis. The trough is the manifestation of the Saharan heat low on the synoptic time scale and confined to 850 hPa and below. The northern wave pouch also has a shallow structure and does not extend to 700 hPa. The southern wave is visible as an elongated closed circulation at 700 hPa along 10°N, south of the AEJ axis. Although the associated cyclonic vorticity extends downward to 850 hPa, the wave pouch does not. Also note that there is an extensive anticyclone to the northwest of the southern pouch at 700 hPa.

By 06Z on 1 September, the 850 hPa wave has propagated to 5°W. The vorticity strip along the trough becomes stronger and extends southward. At 700 hPa, the southern wave pouch is now centered at (4°W, 10°N) with cyclonic vorticity extending westward beyond the coast.

At 06Z on 2 September, the elongated wave pouch has split into two distinct closed circulations at 700 hPa, one off the African coast and the other to the east over land. The circulation in the west is stronger (in terms of vorticity) and better defined than the one to its east. Although a closed circulation is still absent at 850 hPa for the southern wave, the cyclonic vorticity signal has strengthened. Meanwhile, the 850 hPa wave continues propagating westward and begins to exit the African coast.

By 06Z on 3 September, the 700 hPa pouch south of the jet has moved to (22°W, 12°N) and becomes more circular. The 850 hPa wave has extended across the AEJ axis. The centers of the two disturbances are about 4 degrees apart from one another. Meanwhile, the anticyclone in the northwest also propagates westward and is now located on (33°W, 24°N) at 850 hPa. The anticyclone helps to enhance the easterly jet off the coast, and the associated northeasterly flow steers the northern disturbance southward and helps create the favorable environmental flow for the merger of the two disturbances.

At 06Z on 4 September, the 850 hPa pouch and the 700 hPa pouch are less than 3 degrees apart, and the pre-Isabel disturbance now has a deep pouch. This time is thus defined as the merger time. The disturbance keeps intensifying and becomes well aligned vertically at 06Z on 5 September. It developed into a tropical cyclone at 00Z on 6 September. This substantial intensification following the merger time is a typical evolution feature for merger developers. Genesis occurs about 32 hours after merger on average.

Moisture and Convection

To augment the dynamic evolution, the time sequences of relative humidity (RH) and IR brightness temperature with 2.5-day low-passed streamlines are shown in Fig. 3.4 and Fig. 3.5, respectively, for the same time period as in Fig. 3.3. The most evident broad

scale feature in Fig. 3.4 is the moisture contrast over Africa. At 850 hPa, the AEJ axis roughly separates the dry air (RH<40%) in the north from the moist air (RH>60%) in the south. This moisture transition zone around the jet axis is perturbed by synoptic or mesoscale disturbances (Cook 1998; Fink et al. 2004). Also note that the moist air extends farther northward at 850 hPa than 700 hPa due to the prevailing southwesterly monsoonal flow. The northern 850 hPa disturbance remains dry and convection-free over land from 06Z 31 August to 06Z 2 September, with RH ~30% in the vicinity of the pouch, while the southern wave pouch is rather moist, with RH 80% or greater. The southern wave is associated with a mesoscale convective system (MCS), and active convection is also present along the coast. The latter likely contributes to the strengthening of the wave near the coast on 2 September.

From 06Z 2 September to 06Z 3 September, the 850 hPa pouch propagates to the Atlantic and approaches the 700 hPa circulation. The 850 hPa pouch is initially dry after moving over water. Although the 700 hPa pouch is surrounded by relatively dry air immediately to its north and west, the inner pouch region remains moist. Meanwhile, convection associated with the wave is enhanced significantly due to the interaction between the wave and the coastal convection (Berry and Thorncroft 2005), and the 850 hPa wave pouch is moistened substantially in the following 24 hours. This suggests that the positive impacts of vorticity interaction exceed the negative impacts of dry air on convection.

After the two disturbances completely merge on 3 September, the 850 hPa pouch is now vertically aligned with the 700 hPa pouch and has become quite moist by this time (RH>70%). Convection is better organized within the wave pouch (Fig. 3.5), and a tropical

cyclone forms on 6 September. It is noticeable between 06Z on 4-September and 06Z on 5 September that dry air (RH<40%) is advected southward west of the wave pouch at 700 hPa but does not penetrate the inner pouch region. As shown later, this is a critical difference between merger developers and non-developers.

3.4 Merger and Non-Merger Developers

3.4.1 Wave Structure

To illustrate the evolution of non-merger and merger developers, the latitude-height cross section of vorticity (contours) and the Okubo-Weiss parameter (OW) (shading) are shown in Fig. 3.6 from three days prior to genesis (-72 h) to the genesis time (0 h). To highlight the wave structure, vorticity is derived from the 2.5-9 day band-pass filtered data. Since OW is a nonlinear function of the wind field, OW is first derived from the 2.5-day low-pass filtered and 9-day low-pass filtered data separately, and then the difference is taken to produce accurate 2.5-9 day band passed OW and is shown in Fig. 3.6 to represent the wave structure. Both vorticity and OW are averaged over 7 degrees in longitude around the pouch center. Three days prior to genesis, two disturbances are evident in both composites. The two circulation centers are about 10 degrees apart, and the northern disturbance is much weaker and shallower in both composites. There are some noticeable differences between the two composites. First, the southern wave in the non-merger developer composite is stronger than that in the merger composite, and the large values of vorticity extend farther downward from the jet level (~700 hPa). It is possible that a wave pouch has formed at 850 hPa before the wave moves over to the ocean (see Fred (2009) in Wang et al. 2010). Second, the northern vortex in the merger developer composite has stronger cyclonic vorticity and is more closely “connected” to the southern wave in terms

of vorticity distribution. From t=-72 h to t=-48 h, the southern wave intensifies in both composites, but is still stronger in the non-merger composite. The northern vortex remains weak and well-separated from the southern wave in the non-merger composite, but it strengthens and moves southward in the merger composite from t=-72 h to t=-48 h. On average the merger occurs 32 h prior to genesis, or between the t=-48 h and t=-24 h composites. At t=-24 h (shortly after the merger time), the southern wave in the merger composite is centered at 12°N and has intensified significantly, becoming even stronger than the non-merger composite. The large OW values extending down to the boundary layer suggest that a wave pouch may have formed near the surface. Both composites show further intensification in the final day leading up to genesis. In summary, the merger developers start with a weak and shallow wave south of the AEJ, and the merger between the northern wave and the southern wave leads to a stronger and deeper wave pouch, which is consistent with what we have observed in Figs. 3.3-3.5.

3.4.2 Mean States

The mean states for the merger and non-merger developers are examined next. The mean 925 hPa potential temperature averaged over three days prior to genesis is shown in Figure 3.7, along with 600 hPa 9-day low-passed zonal wind. Here the 925 hPa potential temperature is chosen because it can best illustrate the heat low and the low-level meridional temperature gradient over Africa, which is closely associated with the intensity and location of the AEJ. The warm air mass is evident over Africa (Figs. 3.7a and 3.7b) in both composites, but it extends farther westward to the East Atlantic for merger developers (Fig. 3.7c), which helps to maintain the meridional temperature gradient. Consistent with the potential temperature distribution, the easterly jet is stronger and extends farther

westward over the East Atlantic in the merger developer composites (Fig. 3.7c). The statistically significant warm anomalies (above 95% confidence level) over the East Atlantic are also accompanied by an anomalous anticyclone (not shown). Pytharoulis and Thorncroft (1999) showed that the zonally elongated potential temperature gradient is confined to near the coast and curves northward following the coastline in the climatological mean. The weakening of the potential temperature gradient off the coast may lead to the weakening or northward propagation of some northern waves, which tend to follow the strong potential temperature gradient. The westward extension of the hot air mass and the enhanced potential temperature gradient off the coast may help to maintain the northern waves and lead to a better chance for wave merger.

3.5 Merger Developers and Non-Developers

3.5.1 A Typical Non-Developing Merger Case: P22L (2011)

Tropical wave P22L (following the disturbance names at the pouch tracking website (http://www.met.nps.edu/~mtmontgo/storms2011.html) in 2011 was chosen to highlight the typical evolution of a merger non-developer. The wave phase speed average between the 700- and 850-hPa levels is -7.1 m s^{-1} in the zonal direction. A pouch in the precursor wave disturbance can be tracked back 228 hours prior to merger at 700 hPa. Fig. 3.8 shows the evolution of relative vorticity and relative humidity from two days before the merger (12Z 29 August) to two days after the merger (12Z 2 September) at 48 h increments. Streamlines are shown in the co-moving frame of reference.

Two days prior to the wave merger (12Z 29 August), a pouch is visible at 700 hPa south of the AEJ axis centered on (8°W, 11°N). A tripole pattern is visible at 700 hPa with anticyclones positioned northwest (20W, 20N) and northeast (2°W, 20°N) of P22L. Dry

air is associated with the two anticyclones at 700 hPa, but the cyclonic wave pouch south of the jet is quite moist (RH>80%). The cyclonic pouch, however, does not extend down to 850 hPa. A wave trough at 850 hPa is discernible below the 700 hPa wave pouch. In this case the northern wave does not have a closed circulation. A dry trough extends from 25°N to 15°N between 10°W to 20°W north of the jet.

By 12Z on 31-August at the merger time, the 700 hPa wave has propagated to (18°W, 13°N). At 850 hPa the northern disturbance has merged with the southern wave and created a pouch slightly north of the 700 hPa pouch. The initially dry northern wave moistened as it moved south across the AEJ axis, which is typical at low levels for both merger developers and non-developers. The anticyclone over West Africa is still centered near the prime meridian but expands westward, while the anticyclone to the northwest of the pouch has propagated about 15 degrees westward. Due to the southeasterly flow associated with the anticyclone over the land, the 700 hPa wave pouch moves slightly northward into the deformation zone between the two anticyclones. Although the pouch circulation is still moist, the northerly flow associated with the anticyclone to its northwest advects dry air southward into the vicinity of the wave pouch.

Two days after the merger time, the 850 hPa pouch remains moist but the 700 hPa circulation (centered at 32°W, 13°N) has become less well-defined. The pouch is embedded in an amplified wave trough at 700 hPa, and the northerly flow west of the pouch center advects dry air from the subtropics to the pouch periphery. Previous studies have suggested that mid-level dry air reduces cloud buoyancy and suppresses deep convection (e.g., James and Markowski 2010; Kilroy and Smith 2013; Wang 2012). In addition to the impacts of dry air, the vertical displacement of the circulation in the wave increases after

this time. The 850 hPa circulation moves southwest while the 700 hPa wave propagates northwest, resulting in continued dissipation of the wave (not shown).

3.5.2 Developing vs. Non-Developing Merger Composite Analysis

To better understand the processes hindering storm development, Figure 3.9 shows the time sequence of the 700 hPa streamlines and relative humidity composites for developing and non-developing mergers from 48 hours before to 24 hours after merger. Two days prior to merger, the southern wave pouches in both composites are located near the coast. The merger non-developer pouch center (13°W, 11°N) is about 5 degrees westward compared to the developer composite (8°W, 10°N). An anticyclone is present in both composites to the northwest of the wave pouch over the Atlantic. Another anticyclone, which is weaker, is present to the northeast of the wave pouch in the non-developer composite, similar to what is shown in Fig. 3.8. In the developer composite, a ridge extends eastward over land from the anticyclone off the coast.

One day later (t=-24 h), the anticyclonic circulation over land becomes stronger in the merger non-developer composite relative to the developer composite, and the wave pouch is thus sandwiched between the two anticyclones. Due to the steering effect of the northeastern anticyclone, the wave pouch has moved slightly northward to (18°W, 13°N). The wave pouch in the developer composite is centered at (14°W, 10°N), to the south of the anticyclone and the associated eastward extending ridge axis.

At the merger time, the merger non-developer pouch has moved northward to (22°W, 15°N), and the associated cyclonic vorticity weakens substantially (not shown), resulting in a size reduction of the wave pouch. In contrast, the developing pouch is centered on (21°W, 12°N) and starts to take a more circular shape. A sharp contrast

between the developers and non-developers at this time is the anticyclones north of the wave pouches. In the developer scenario, the anticyclone to the northwest maintains a strong circulation, and a second anticyclone to the northeast has developed with a distinct center. The twin anticyclones haven't split yet (no strong northward wind between them) and help to keep the pouch in the southern wave track. In the non-developer composite the anticyclone to the northwest has weakened to a ridge and transports dry air into the pouch circulation, similar to P22L (2011) at 12Z 02 September (Fig. 3.8).

One day after the merger time, the tripole pattern in the developer composite becomes more pronounced, with the wave pouch centered between the anticyclones near (27°W, 12°N). For the non-developers, an open ridge, which results from the decayed northwestern anticyclone, advects dry air west of the wave trough. Meanwhile the northeastern anticyclone (15°W, 19°N) remains prominent and continues to steer the pouch northward. The wave pouch is centered near (29°W, 15°N). The composite sequence of the non-developers is similar to what is shown for P22L in Fig. 3.8.

To examine the pouch evolution, Fig. 3.10 shows the time-height cross section of relative vorticity, relative humidity and vertical shear for the merger developers and non-developers. The profiles of relative vorticity (Figs. 3.10a and 3.10b) for developers and non-developers are similar prior to the merger time (t = 0 h) except that the former is slightly stronger, especially between -24 and 0 h. With the merger of the two disturbances, the cyclonic vorticity extends downward in both composites. Vorticity strengthens substantially in the developer composite in the following two days but weakens significantly for non-developers after 12 h. The striking difference in relative humidity (Figs. 3.10c and 3.10d) between the developers and non-developers is the drying for the

non-developers after t = 0 h above 800 hPa, with the most pronounced drying between 200-500 hPa (RH down to less than 35%). Figures 3.10e and 3.10f show the vertical shear at different levels with respect to 700 hPa. Compared to the developers, the non-developers have relatively weak shear below 700 hPa, especially after t = 0 h, but they are subject to stronger vertical shear above 500 hPa.

To put the differences in RH and vertical shear in a proper synoptic-scale context, the 400 hPa RH and streamlines are shown in Fig. 3.11. The developers are characterized by a small but well-defined closed cyclonic circulation, with the center slightly to the west of the 700- hPa pouch center (which is the center of the domain). Although dry air wraps around the cyclonic circulation northwest of the pouch center, the pouch region is quite moist and embedded in a zonally elongated moisture zone, which is likely the ITCZ. The 400 hPa flow of the non-developers features a broad and deep trough, extending beyond 15 degrees latitude north of the 700 hPa pouch. The trough axis is about 5 degrees to the west of the 700 hPa pouch center. The spatial scale of the trough is much larger than that of the 400 hPa pouch of the developers, and the northerly flow advects dry air from the subtropics. The broad trough is more succinctly shown in the difference between developers and non-developers (Fig. 3.11c). The dry air west of the wave pouch is collocated with the southerly flow of the trough. Moreover, the westerly anomalies associated with the trough explain the stronger westerly vertical shear in the upper troposphere, and the westerly flow spreads dry air eastward toward the pouch circulation.

Fritz and Wang (2013) suggested that dry air can be transported from the upper troposphere to the middle troposphere and hinder the storm development. To examine whether this is the case, Figure 3.12 shows the vertical cross section along the center

latitude of the 700 hPa pouch. Prevailing westerly relative flow is found in the upper troposphere for non-developers, while the relative flow is much weaker for developers. Figure 3.12 also shows that the dry air is accompanied by subsidence in the middle to upper troposphere. The dry air ahead of the wave pouch in the upper troposphere is consistent with Hopsch et al. (2010), who attributed the non-development of an AEW near the coast to the presence of mid- to upper-level dry air just ahead of the AEW trough. The presence of the upper-level trough was also discussed by Arnault and Roux (2010). They suggested that a midlatitude trough approaching from the northwest contributed to the weakening of the wave.

As mentioned in the introduction, dry air has two major sources over the Atlantic: the SAL and midlatitude intrusion. Figure 3.12 suggests that the 700 hPa dry air at least partly originates from the upper troposphere and is associated with dry air intrusion from the middle latitudes. To further test this idea, we examine the dust distribution using the AOD from the MODIS Level 3 products (Hubanks et al. 2008). Data from the Terra and Aqua satellite platforms are processed separately. As sun-synchronous satellites, Terra (descending orbit) passes the equator near 10:30 am (local time) and Aqua (ascending orbit) passes the equator near 1:30 pm (local time). For each merger system, the MODIS observations are first searched from 24 h before to 24 h after the merger time, which lead to 2 Terra observations and 2 Aqua counterparts. The pouch locations are then derived for each satellite passing time using the linear interpolation, and composites are constructed with respect to the pouch center. Streamlines are constructed in a similar way using linear interpolation. The AOD composites, superimposed on streamlines, are shown in Fig. 3.13. The streamlines appear to be a transition from t=-24 h to t=0 h (Fig. 3.9). Dust is present

in the vicinity of the wave pouch in both composites. Although large AOD values are observed in the developer composite, they do not penetrate the inner pouch region. In contrast, AOD > 0.4 is present in the northwest quadrant of the wave pouch in the merger non-developer composite. It is interesting to note that the AOD values are smaller in the non-developer composite than in the developer composite despite the more pronounced dryness in the former. This suggests that the dry air in the non-developer composite can not be simply attributed to the SAL, and it also suggests that the presence of the SAL near the wave pouch does not necessarily hinder the storm development, which is consistent with Braun (2010)'s finding about the impacts of the SAL on tropical cyclone intensification. We also carried out backward trajectory analysis for several non-developers using the Hybrid Single Particle Lagrangian Integrated Trajectory Model (HYSPLIT) model (Draxler and Hess 1997, Draxler and Hess 1998, Draxler 1999). The trajectories suggest that dry air originates both from West Africa and from the midlatitudes (not shown).

3.6 Summary

Previous studies have identified two groups of waves over West Africa, one to the south and the other to the north of the African Easterly Jet (AEJ) (e.g., Reed et al. 1988; Pytharoulis and Thorncroft 1999; Thorncroft and Hodges 2001). The two groups of waves have different structures. The southern waves are moist and propagate along the zone of strong PV gradient, peaking around the jet level. In contrast, the northern waves are dry and confined to 850 hPa and below, propagating along the strong meridional gradient of potential temperature. A northern wave sometimes merges with a southern wave near the coast of West Africa. The dynamic and thermodynamic evolution of the waves during the

merger and the impacts of mergers on the subsequent storm development are examined in the framework of the marsupial paradigm in this study.

Three groups of storms are identified: non-merger developers, merger developers, and merger non-developers. Here a northern wave is defined as a propagating cyclonic vorticity feature north of the AEJ, and the merger time is defined as the time at which the horizontal distance between the northern wave (850 hPa) and the southern wave pouch (700 hPa) is 3 degrees or less. Only a small fraction of mergers (~20%) intensify into tropical cyclones over the East Atlantic, and they account for 31% of the Cape Verde storms.

A case study is used to illustrate the typical evolution sequence for a merger developer, Isabel (2003). Along with composite analyses, it is shown that merger developers start with a shallower and weaker wave pouch. The northern wave moves southwestward and merges with the southern wave pouch near the coast of West Africa. Although the northern wave is initially dry, it is typically moistened quickly, which is often associated with coastal convection. The merger of the two disturbances leads to a stronger and deeper wave pouch, and a Cape Verde storm forms 32 h later, on average. A deep pouch has been suggested as a necessary condition for tropical cyclogenesis (Wang et al. 2012). The analysis thus suggests that the dynamic interaction of two disturbances creates a more conducive structure for tropical cyclone formation. It is also found that merger developers are related to a stronger and more extensive Saharan heat low. Due to the enhanced meridional temperature gradient, the AEJ extends further westward over the East Atlantic, which creates a more favorable environmental condition for the maintenance and propagation of the northern waves.

Merger developers and non-developers are also compared to investigate the processes that hinder the storm development. The composites of the two groups resemble each other prior to the merger time. The 700 hPa circulation is characterized by a tripole pattern prior to merger, with anticyclones positioned to the northwest and northeast of the wave pouch. This pattern is maintained until genesis for merger developers, but the anticyclone to the northwest breaks down to an open ridge shortly after merger. The ridge advects dry air from north, while the anticyclone to the northeast steers the wave pouch slightly northward. In contrast, the tripole pattern for merger developers helps keep the wave pouch in a zonal track and the wave pouch remains moist. Although merger leads to a stronger wave pouch in both cases, the developers keep intensifying while the non-developers weaken after merger in terms of vorticity evolution.

The weakening of the non-developers can be attributed to strong westerly upper-level shear relative to 700 hPa and dry air intrusion in the middle to upper troposphere (200-500 hPa). The dry air and enhanced shear are associated with a strong and broad upper tropospheric trough to the west of the low-level wave pouch. The upper-level trough advects dry air from the extratropical Atlantic and induces strong westerly vertical shear. The middle to upper-tropospheric dry air is collated with subsidence and may be transported to the lower troposphere. Composites of AOD show that merger developers were associated with higher AOD values, despite the fact that the non-developers have much drier air in the vicinity of the wave pouch. This suggested that the dry air can not be simply attributed to the Saharan Dust Layer. Instead, it at least partly originates from the midlatitude and from the upper troposphere.

3.7 Figures

Storm Type	Merger Lon	Merger Lat	Genesis Lon	Genesis Lat	Sample size	Time period (yr)	Number of storm per year
Developing Merger	21.2W	12.1N	27.8W	12.7N	18	22	0.82
Developing Non-Merger	-	-	28.2W	12N	51	22	2.32
Non-Developing Merger	22.3W	14 .7N	-	-	16	5	3.2

Figure 3.1. Statistics on the defined storm groups.

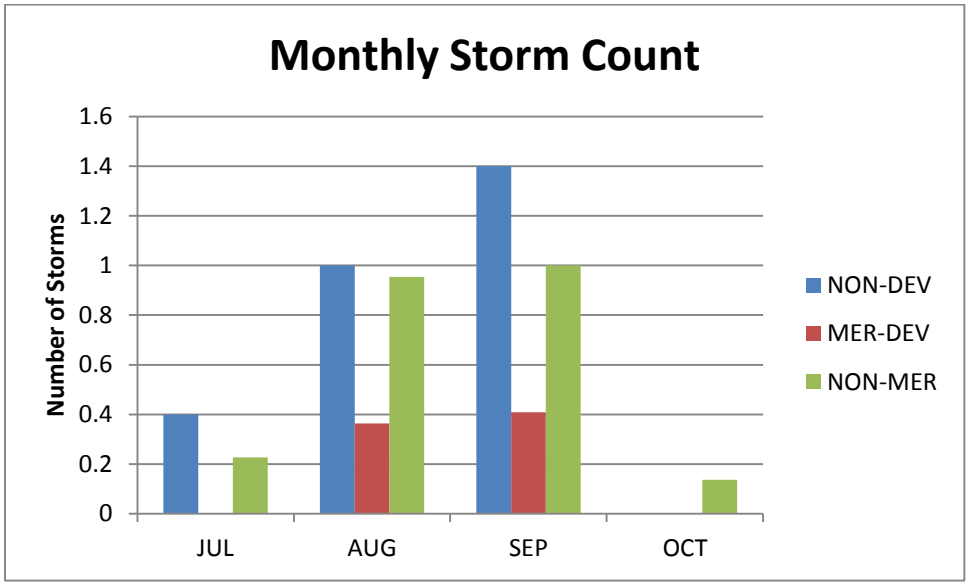

Figure 3.2. Total storm numbers by month and category, normalized per year.

Isabel (2003) VORT and UV

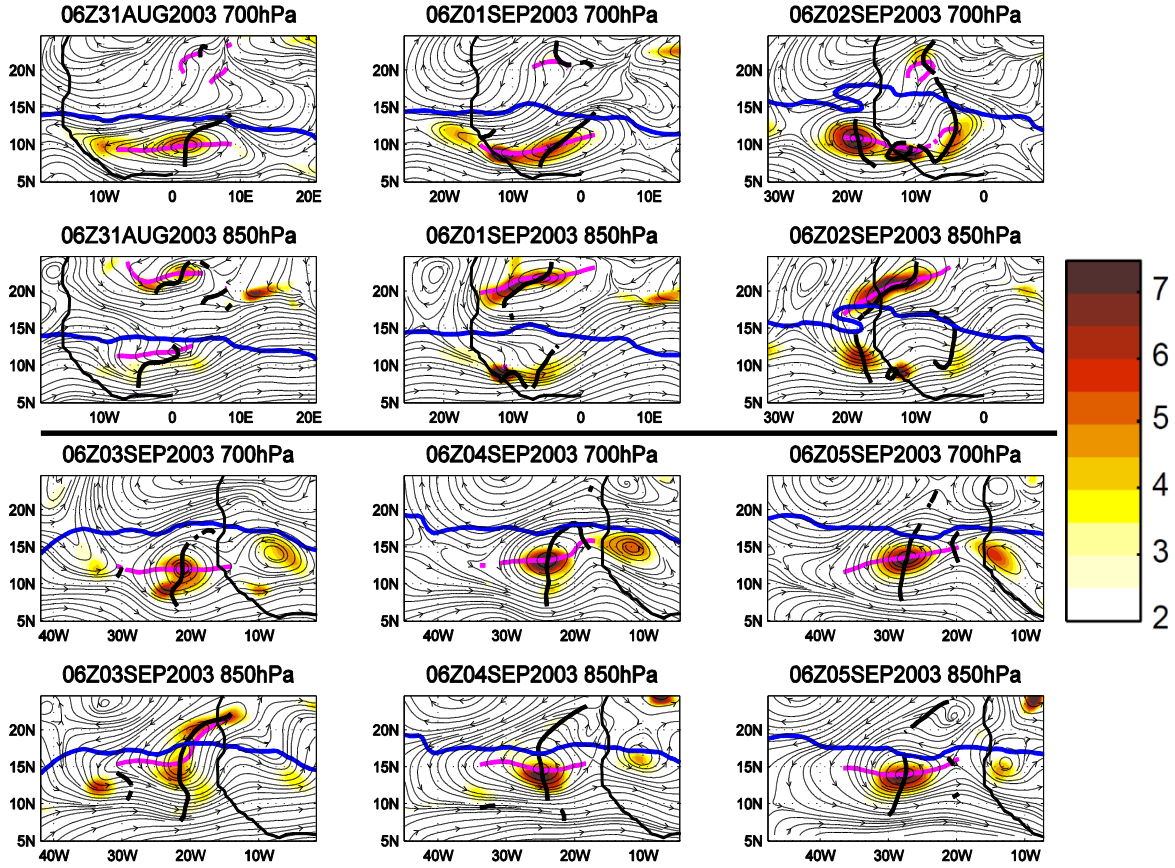

Figure 3.3. Evolution of Isabel, 2003 with 2.5 day low-passed data for vorticity (10^{-5} s^{-1}) and co-moving streamlines. Also included are the wave trough axis and critical layer, denoting pouch center at the intersection points. AEJ axis is shown in blue contours. The wave trough is drawn through the region of cyclonic vorticity where V=0 m s^{-1}, and the same is done for the critical layer, but for U=0 m s^{-1} instead. Highlights key features of the merger process for a representative individual case.

Isabel (2003) RH and UV

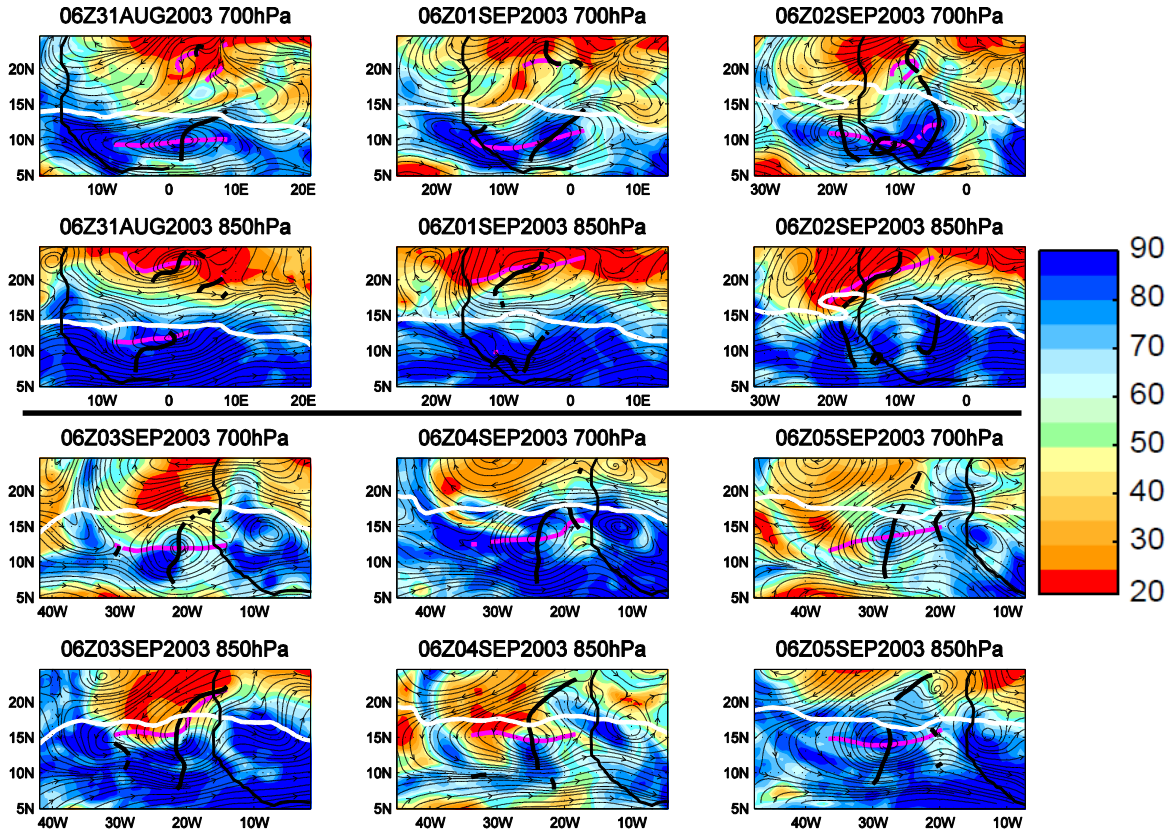

Figure 3.4. Evolution of Isabel, 2003 with relative humidity (%) and 2.5 day low-passed co-moving streamlines. Also contoured are the wave trough axis (black) and critical layer (magenta), denoting pouch center at the intersection points. Plots are centered on the wave pouch center at 700 hPa. The AEJ axis is shown with a white contour.

Isabel (2003) IR and 700 hPa UV

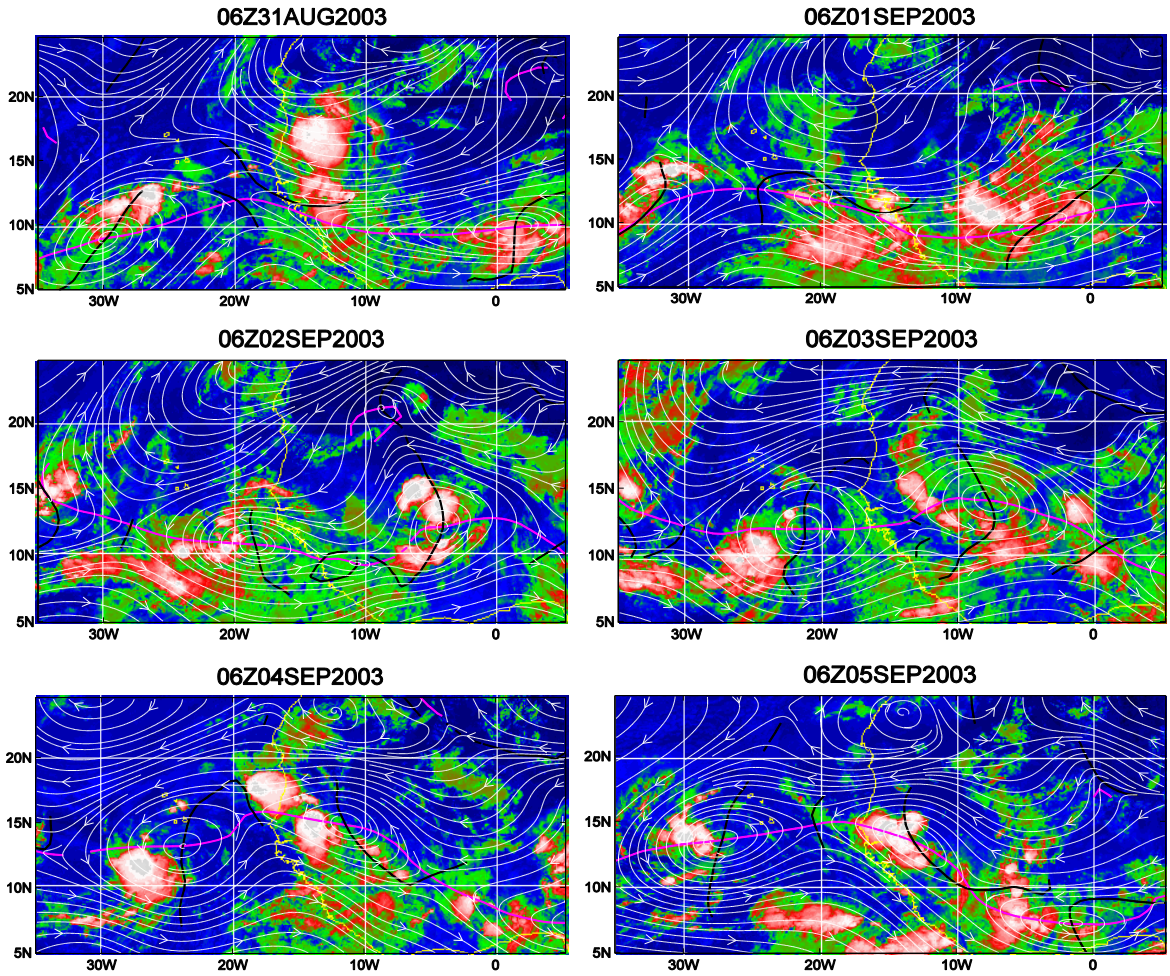

Figure 3.5. Evolution of Isabel, 2003 with satellite IR and 2.5 day low-passed streamlines at 700 hPa over a fixed domain in the co-moving frame of reference. Also shown are the wave critical layer (magenta) and trough axis (black) in contours.

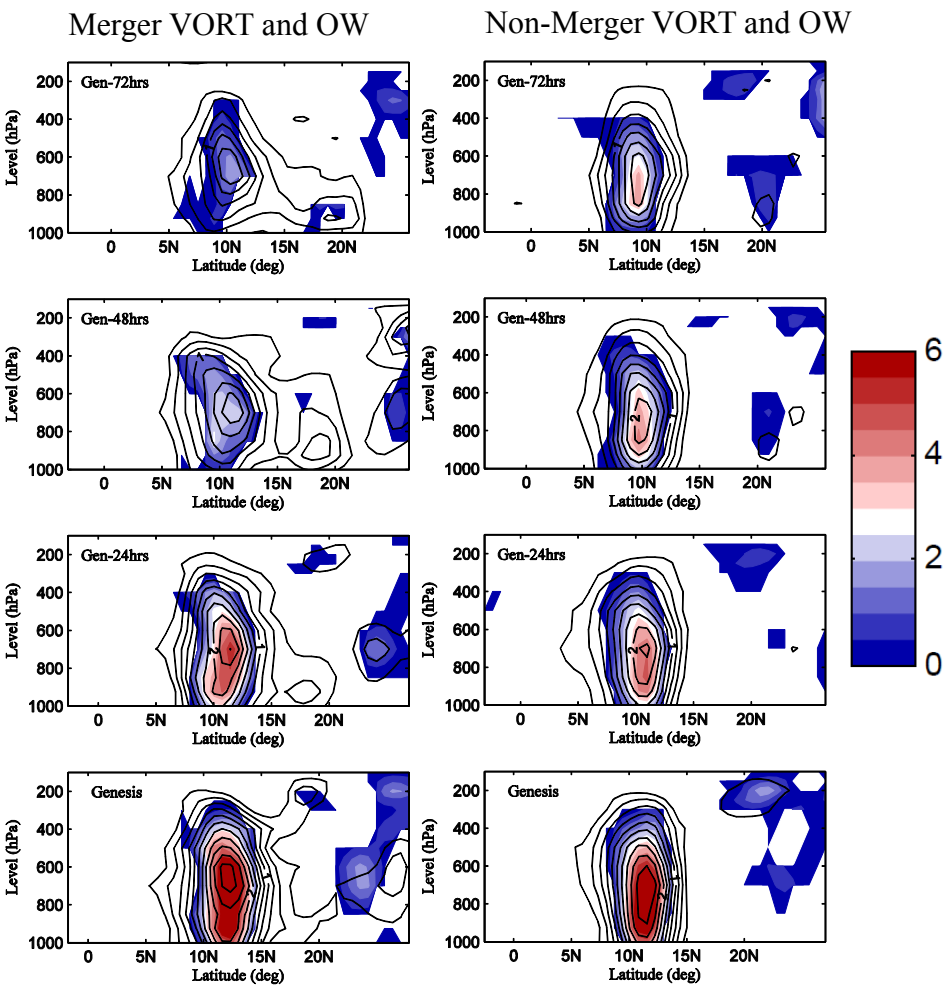

Figure 3.6. 2.5-9 day band-pass filtered Okubo-Weiss parameter (shading, 10^{-10}) and vorticity (contours). Labels on contours correspond to 10-5 s^{-1}, and are at a $.25*10^{-5}$ s^{-1} interval. Data shown represent a 7 degree latitudinal cross section, centered on the 700 hPa pouch center.

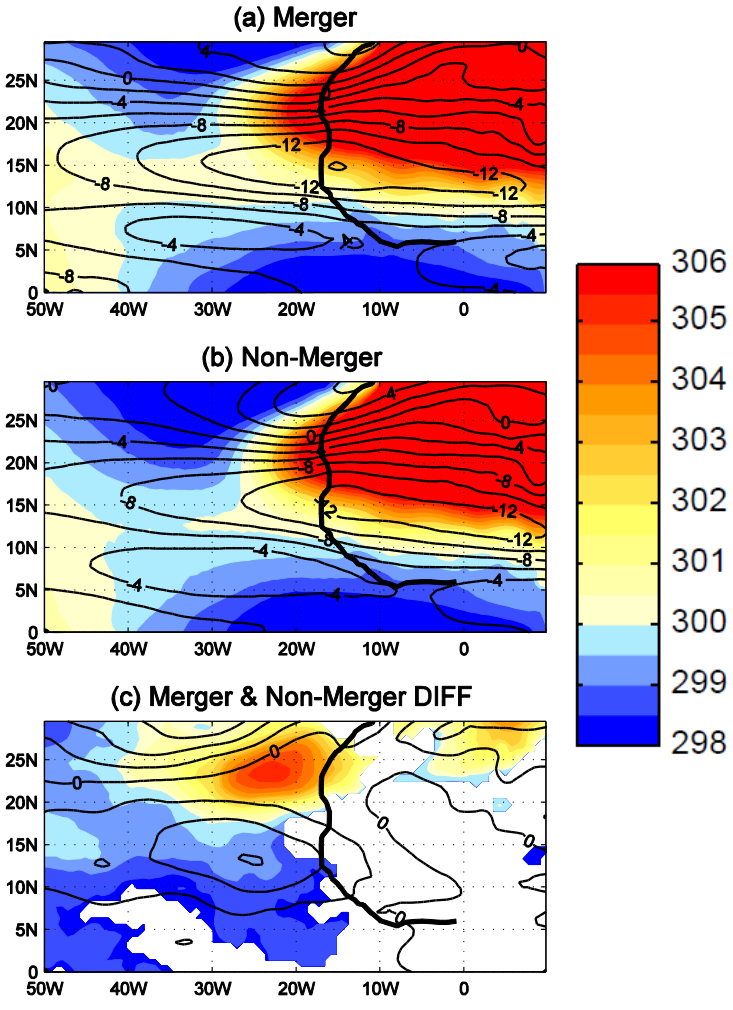

Figure 3.7. 925hPa potential temperature (K) with 9-day low-passed 600hPa UWIND. In the difference plot, only statistically significant differences are shown for the temperature.

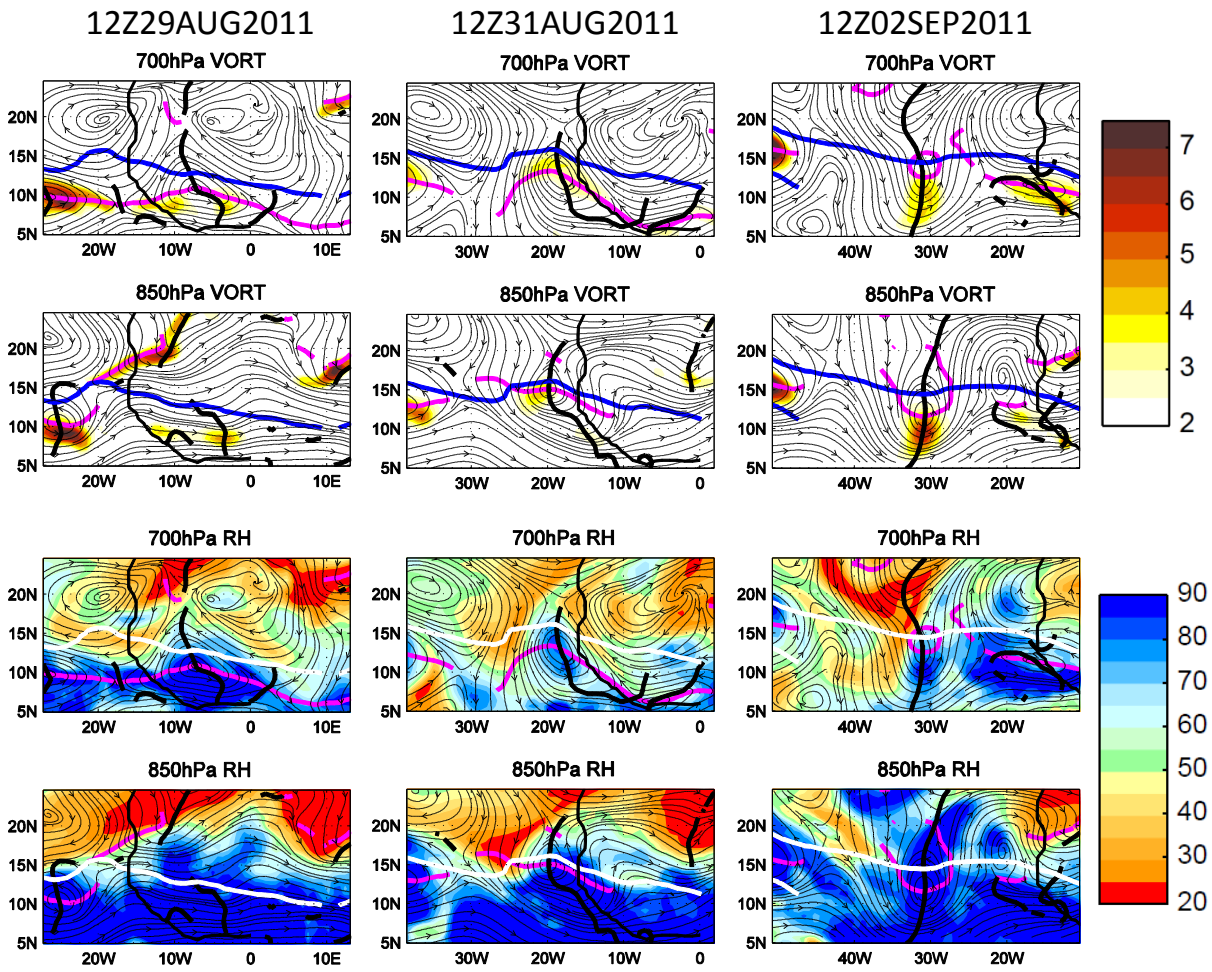

Figure 3.8. Case study for P22L at 48 hour intervals, starting two days prior to merger. The top two rows display 2.5 day low-passed 700 and 850 hPa vorticity (10^{-5} s^{-1}), and the bottom rows display relative humidity at the same levels from 20 (blue) to 90 (red) percent. All plots include co-moving streamlines, the wave critical layer (magenta), wave trough axis (black), and AEJ axis (blue).

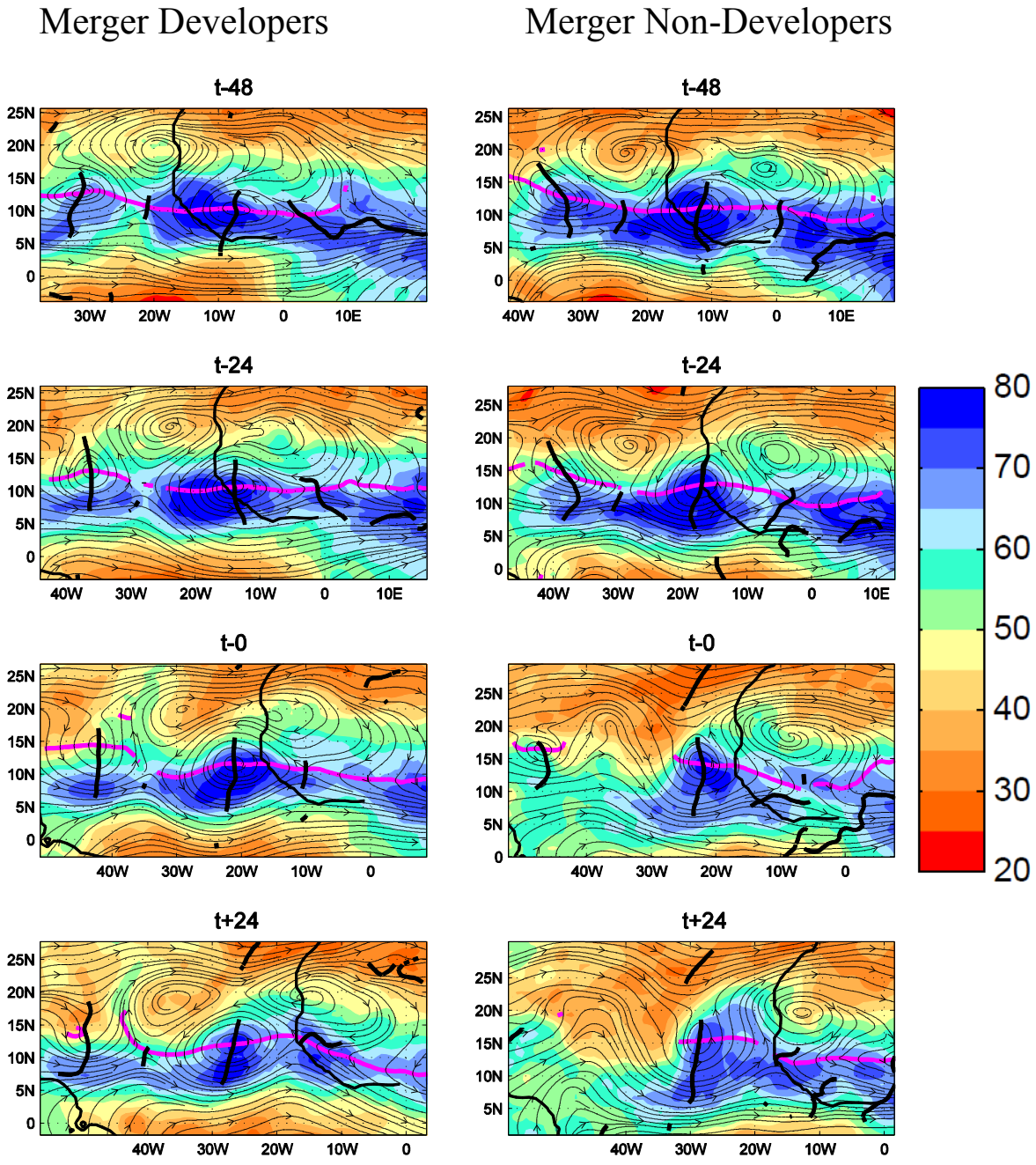

Figure 3.9. Composite means for merger developers and non-developers. Displayed are relative humidity (%), and total wind field data for streamlines in the co-moving frame of reference at 700 hPa. Also plotted are the wave trough axis in black, wave critical layer in magenta, and continental coastlines.

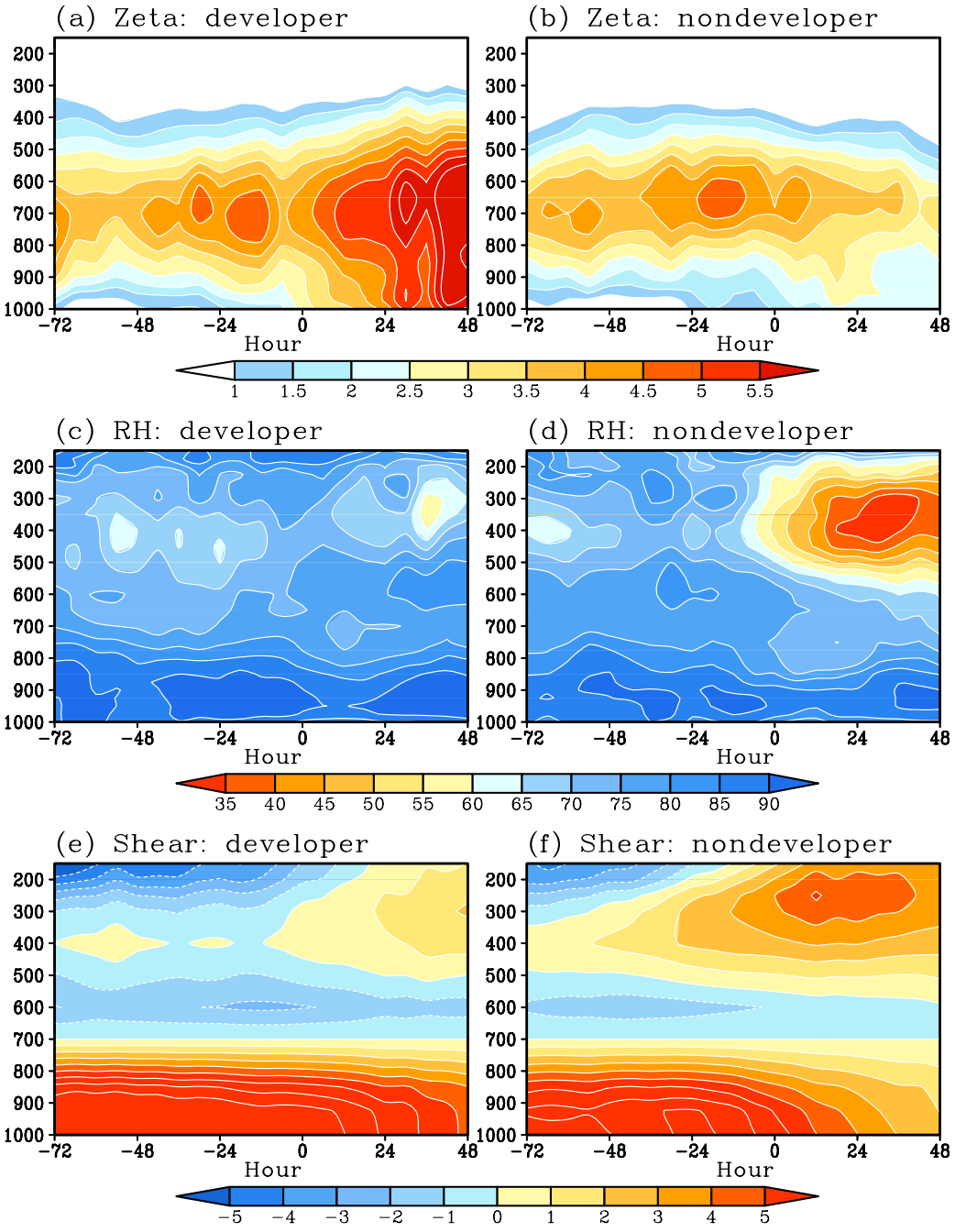

Figure 3.10. Time-height cross section of relative vorticity (zeta; top; units: s^{-1}), relative humidity (RH; middle; units: %) and vertical shear relative to 700 hPa (bottom; units: m s^{-1}) from 72 hours before to 48 hours after merger. The left column is for merger developers and the right column for merger non-developers. Unfiltered data were used to derive all variables. Relative vorticity and relative humidity are averaged over a ~1.4-degree square box to represent the inner pouch region, and vertical shear is averaged over a ~10-degree square box to represent the environment.

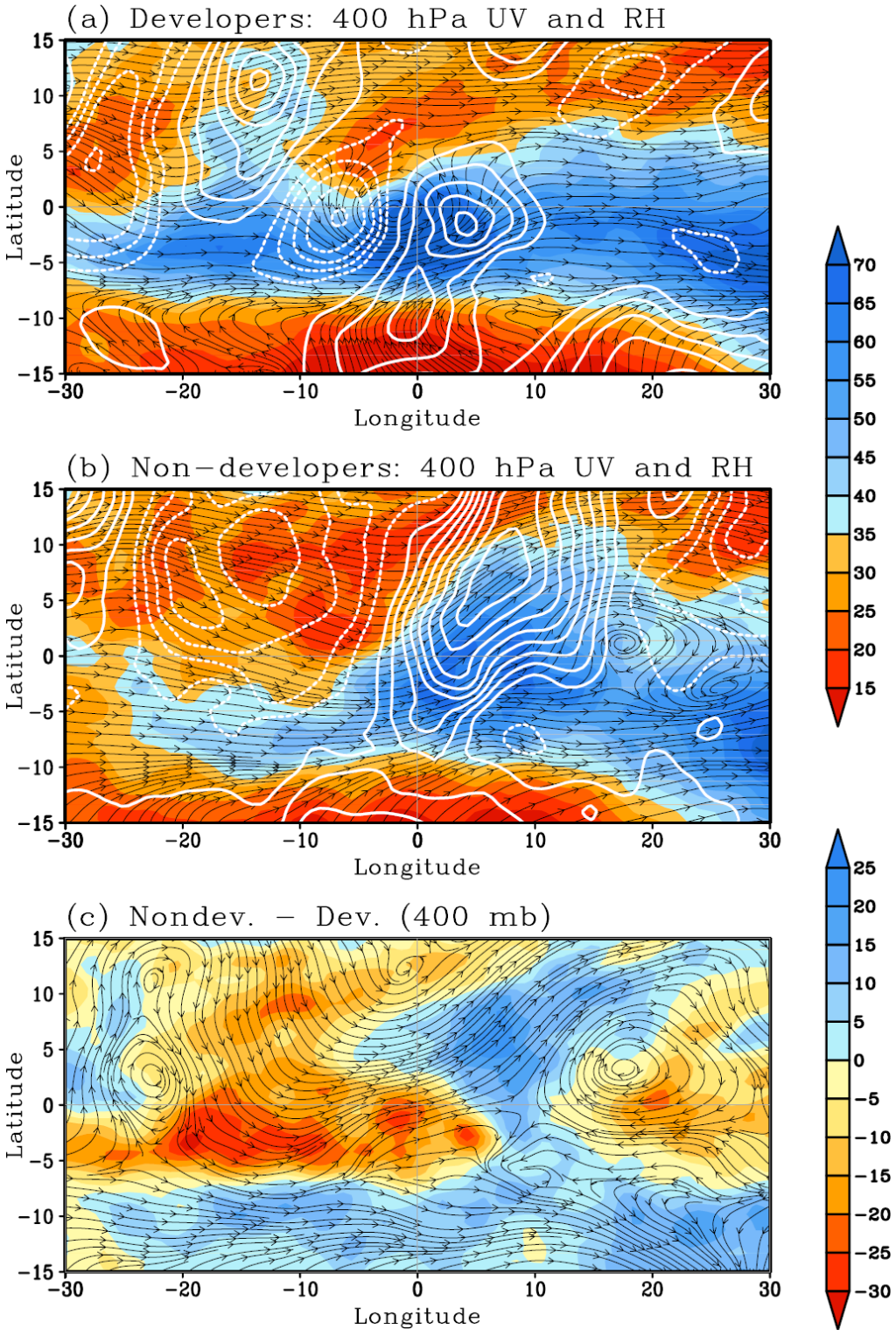

Figure 3.11. 400-hPa streamlines and relative humidity (shading) for (a) merger developers, (b) merger non-developers and (c) their differences. The white contours in (a) and (b) are 400 hPa meridional wind. The domain is centered at the 700 hPa pouch center.

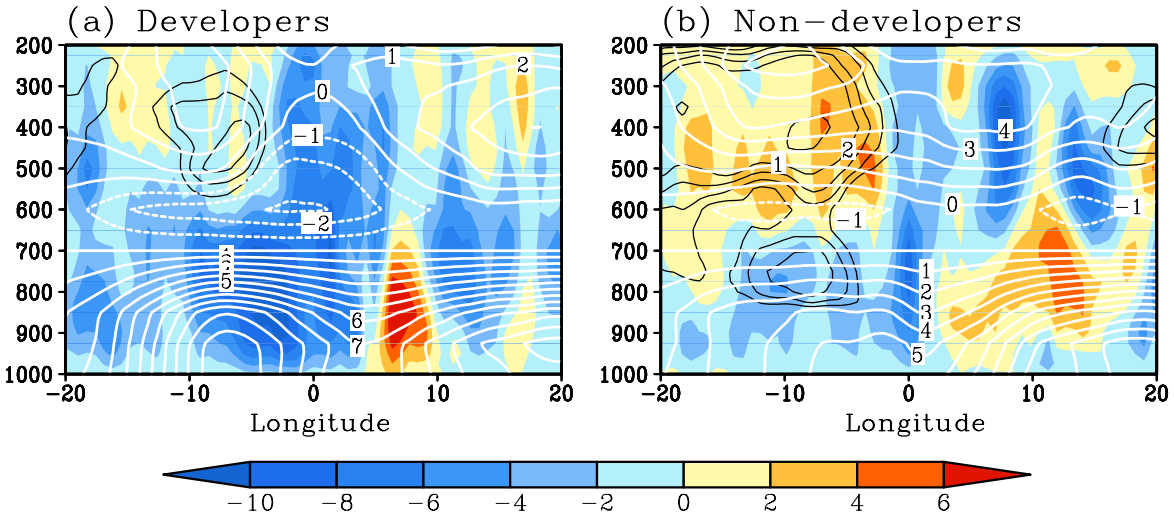

Figure 3.12. Vertical cross of vertical velocity in isobaric coordinates (shading; units: hPa s^{-1}), relative humidity less than 50% (black contours with intervals 5%) and vertical shear of the zonal wind relative to 700 hPa (white contours) for merger (a) developers and (b) non-developers. The cross section is along the center of the 700-hPa pouch. Vertical velocity and relative humidity are from unfiltered data, and zonal wind are 2.5-day low-pass filtered. The zero longitude indicates the pouch center location.

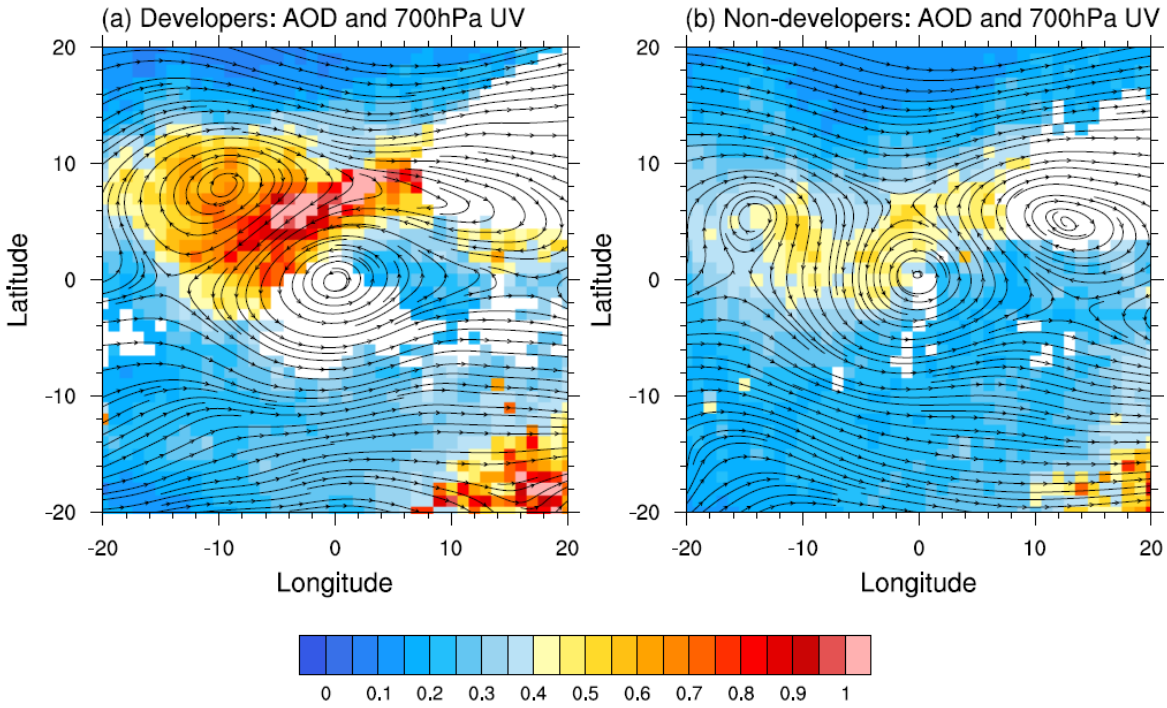

Figure 3.13. Composites of 700 hPa streamlines and aerosol optical depth (AOD; shading) for merger (a) developers and (b) non-developers. The domain is centered at the 700 hPa pouch center. To ensure the robustness of the composites, AOD are not shown at grid points where more than 80% of the samples are affected by cloud contamination.

Chapter 4: Interannual Variability of Middle and Upper Tropospheric Dry Air and Its Impacts on Tropical Cyclone Activity over the Atlantic Basin

4.1 Introduction

The diagnosis in chapter 3 suggests that dry air in the middle and upper troposphere may have impacts on tropical cyclone formation. In this chapter we will examine in detail the interannual variability of the middle to upper troposphere dry air and its impacts on Atlantic tropical cyclone activity. We will investigate the following specific issues:

- the interannual variations of dry air occurrence over the Atlantic Ocean;
- their relationship with the large-scale circulation;
- the possible impacts on the variability of the Atlantic tropical cyclone activity;
- the origin of dry air.

Since relative humidity does not follow a Gaussian distribution, the monthly or seasonal mean can not well represent the variability of relative humidity. Rather, the distributions of humidity exhibit bimodal structures in the middle to upper troposphere (Brown and Zhang 1997), which reflects the occurrences of drought and enhanced convective activity. This bimodal distribution has important radiative effects, resulting in reduced Convective Available Potential Energy (CAPE) for convection due to enhanced longwave cooling in dry periods (Zhang and Chou 1999). Relative humidity can not be adequately represented by the monthly or seasonal mean field due to its bimodal distribution, which highlights the need to define dry air occurrence on the synoptic time scale. Building on the previous work, *we hypothesize that the frequency of occurrence of dry events has an impact on tropical cyclone activity. Additionally, it is expected that dry*

air may originate from the upper troposphere in the subtropical to middle latitudes in association with the large-scale subsidence and synoptic scale anticyclonic flow.

4.2 Data and methods

The six hourly ERA-Interim reanalysis (Simmons et al. 2007) data from 1979-2010 were used to identify the frequency of occurrence of dry air and to conduct empirical orthogonal function (EOF) analysis with associated composites. The layer averaged RH was calculated between 600-850 hPa and 300-500 hPa, respectively, to represent the middle troposphere and upper troposphere. To examine the role of the SAL as a source of dry air, we used the satellite-derived monthly mean dust optical depth (DOD) dataset developed by Amato Evan. These data have a horizontal resolution of one degree and available for 1982-2009 (Evan et al. 2006, Evan and Mukhopadhyay 2010).

Backward trajectories were derived from the HYSPLIT model using the ERA-Interim reanalysis data to determine the origin of dry air. The Best Track data from the National Hurricane Center (NHC) were used to assess the impacts of the dry air occurrence on Atlantic TCs. In addition, the Global Precipitation Climatology Project (GPCP) v2.2 data were used to examine the precipitation anomalies associated with dry air. All analyses presented are taken from August-September, the peak hurricane season over the Atlantic when most tropical cyclones form over the MDR region.

Fig. 4.1 shows the probability distribution of the layer mean relative humidity between 300-500 hPa (upper troposphere) and 600-850 hPa (middle troposphere). The upper tropospheric RH is strongly skewed toward low values, suggesting a low-frequency occurrence of high humidity in the upper troposphere. The mid-tropospheric RH has a bimodal distribution, with a primary peak at 75% and a secondary peak around 50%. Due

to the strong skew (300-500 hPa) or the bimodal (600-850 hPa) distribution of RH, the seasonal mean relative humidity (indicated by the blue line) is quite different from the mode of frequent occurrence and does not adequately represent the variability of the moisture distribution. We thus use the frequency of dry air occurrence to examine the fluctuations of moisture on the subseasonal time scale. A dry air day is identified when two conditions are met continuously for four 6-hourly time periods (one day): 1) relative humidity (RH) is equal to or less than half a standard deviation below the mean and 2) RH is less than a critical value, RHc. RHc is set to 50% for the middle troposphere and 40% for the upper troposphere. The frequency of dry air occurrence is defined as the ratio of the number of dry air days to the total number of days in August and September and is shown as the number of dry air days per season.

4.3 The pattern of dry air frequency

Based upon our definition of dry air occurrence, a 32-year average of dry air days during Aug-Sep for the 600-850 and 300-500 hPa layers is shown in Fig. 4.2. In the middle troposphere, dry air days occur most frequently over the East Atlantic around 20°N (off the coast of West Africa) and extends southwestward to the central Atlantic/Main Development Region (MDR) with an axis near 15°N. The close proximity to the Saharan Desert suggests that these dry air days may be associated with dust outbreaks, which is examined later. In the upper level pattern, a high frequency of occurrence covers the tropical and subtropical Atlantic, with a maximum greater than 22 dry air days over the Central Atlantic. It is noteworthy that both patterns weaken considerably west of the MDR, especially over the Caribbean Sea and the Gulf of Mexico.

The first EOF modes for the middle and upper tropospheric dry air occurrence and the contribution of the first 10 modes to the total variability are presented in Figs 4.3 and 4.4. The first modes explain 23 and 27 % of the total variance for the 600-850 and 300-500 hPa layers, respectively. Both patterns are centered north of the MDR, extending over the East Atlantic and generally peaking between 20-25°N. The temporal correlation between the two EOF time series is 0.39. Although the correlation is above the 95% confidence level, it suggests that one mode can explain only 15% of the total variance of the other mode, and they are therefore independent of each other to some extent. It is also worth noting that the upper-level EOF1 has a dipole pattern, and the variations over the Caribbean and the Gulf of Mexico are opposite to those over the Central and East Atlantic.

4.4 Impacts of middle troposphere dry air occurrence

To assess the impacts that the middle tropospheric dry air occurrence may have on TC activity, the dry air days and tropical cyclone tracks for the six strongest positive years and six strongest negative years of the EOF1 pattern are shown in Figs. 4.5 and 4.6. In Fig. 4.5, many more dry air days occur across and north of the entire Atlantic MDR for the positive phase, while much less dry air days occur over the Caribbean and Gulf of Mexico in both phases. As shown in Fig. 4.7, the 6 positive years have 30 storms and the six negative years have 42 storms, suggesting that this mode significantly impacts the tropical cyclogenesis frequency. In addition, differences are found in the storm tracks and genesis locations. In the negative phase of EOF1, dry air days occur less frequently in the middle troposphere over the tropical and subtropical Atlantic. Consequently, more storms form over the Central and East Atlantic MDR. Furthermore, storm intensities are higher in the negative phase. The negative (positive) phase had a considerably higher (lower) number of

major hurricanes with 13 (6) storms falling into this category (Fig. 7). Cumulatively, the differences between the tropical cyclone tracks reveal significantly reduced tropical cyclone activity over the Central and East Atlantic in the positive phase of EOF1.

To examine the origin of the dry air, composites of dust optical depth were constructed to compare the 5 strongest positive and negative phase years of the EOF pattern (one of the 6 most positive years of EOF1 was outside the dust optical depth data range, which is why 5 years were chosen rather than 6). Fig. 4.8 shows that high DOD occurs between 10-20°N in both composite means, and the composite difference shows significantly higher DOD in most of the MDR in the positive phase of EOF1. Therefore, the Atlantic dust distribution suggests that the SAL contributes to midtropospheric dryness and to the suppression of East/Central Atlantic TC activity.

Another possible source for dry air in the middle troposphere is from the subtropics and midlatitudes in association with subsidence. To examine this possibility, 10-day backward trajectories were calculated using the HYSPLIT. A representative case (12Z 15 Sep, 1994) from the positive phase of the 600-850 hPa EOF1 pattern was chosen, as depicted in Fig. 4.9. The trajectories were initialized at 700 hPa, the middle of the 600-850 hPa layer. A box was selected in the core of the dry air over the MDR near 20°N, and a group of 16 trajectories were initialized at various locations within the box. Fig. 4.9 shows that most trajectories lead back to the subtropical East Atlantic in association with an apparent anticyclone in the upper troposphere and that a few originate over West Africa. This suggests that dry air can be associated with subsidence in an extratropical anticyclone in addition to originating from the SAL. Trajectory analysis was carried out for different

dry events, and when initialized near the coast of West Africa, a larger number of trajectories originate from West Africa than the midlatitude.

The trajectories indicated the importance of large-scale patterns in the distribution of dry air. Based on this indication, 850 hPa heights and streamlines (Fig. 4.10), and 200-850 hPa vertical shear (vector difference; Fig. 4.11) are examined. The different modulation of the 850 hPa subtropical high over the Atlantic is evident between the positive and negative phase years of the 600-850 hPa EOF1 in Fig. 4.10. There is an eastward retreat of the subtropical high in the negative phase years, which contributes to the increasing number of TCs that recurve northeastward over the Central Atlantic. 200-850 hPa shear is also consistent with the configuration of the large-scale flow difference between the positive and negative phase years in Fig. 4.11. Regions of enhanced 850 hPa easterlies west of 40°W between 10 and 20°N are marked by stronger shear in the positive phase years, consistent with reduced TC activity over the region. However, the difference in vertical wind shear (VWS) can not explain the difference in TC activity in the eastern MDR region and the subtropical Atlantic (between 20-30N).

There is potential to improve the understanding and predictability of dry air occurrence if it is related to large-scale climate modes. A correlation of the leading mode of the 600-850 hPa EOF analysis with SST was conducted to evaluate the relationship to SST and some dominant climate modes, such as the Atlantic Meridional Mode (AMM), North Atlantic Oscillation (NAO), and the El Nino Southern Oscillation (ENSO). Midtropospheric dry air was found to have a weak negative correlation (-0.40) with the AMM and with the NAO (-.46), but was not significantly correlated with ENSO (Fig. 4.12). These correlations are consistent with the observed reduction of TCs over the MDR in the

negative phase of the AMM/NAO. Besides dry air, the modulation of vertical wind shear associated with the AMM and NAO may also contribute to the variations of Atlantic tropical cyclone activity.

4.5 Impacts of upper troposphere dry air occurrence

To assess the impacts that 300-500 hPa dry air occurrence may have on TC activity, the composites of the dry air days and tropical cyclone tracks are plotted in Figs. 4.13 and 4.14 for the six most positive and six negative phase years of the EOF1, respectively. Fig. 4.13 shows that dry air days occur more frequently over the Central and East Atlantic but less frequently over the Gulf of Mexico in the positive phase of EOF1. The 6 most positive phase years from EOF1 have 44 storms, and the 6 most negative phase years have 51 storms (Fig. 4.7). Compared to the negative phase, more storms formed near the coast (more landfalling storms) but less over the MDR in the positive phase, and fewer total storms formed over the Atlantic basin. However, no significant impact on TC intensity could be identified from the 300-500 hPa EOF1 in terms of the number of major hurricanes, as 12 (14) such storms formed in the positive (negative) phase. Similar to the midtropospheric pattern, the upper troposphere dry air events act to reduce TC activity over the Atlantic MDR, the region with the highest dry air occurrence.

To examine the linkage of the dry air occurrence in the upper troposphere to dust outbreaks, composites of dust optical depth were constructed to compare the 5 strongest positive and 5 strongest negative phases of the EOF pattern. Similar to Fig. 4.5, Fig. 4.15 shows that dust occurs most frequently between 10-20°N and decreases westward from the coast of West Africa. Interestingly, dust is reduced over the tropical and subtropical North Atlantic in the positive phase of EOF1. This is consistent with Braun (2010), who

suggested that the processes which produce the SAL cause drying below 700~600 hPa and moistening in the 600 to 400 hPa layer. This again confirms that the middle and upper tropospheric dry air occurrences are independent of each other to some extent.

The predominant source for the dry air occurrence in the upper troposphere may be from the subtropics and midlatitudes. To examine this possibility, a representative case was chosen for the 300-500 hPa EOF1 positive phase and displayed in Fig. 4.16. Dry air is visible over the MDR within the box, centered near 15°N. 10-day backward trajectories were initialized within this box using the HYSPLIT model to evaluate the source of dry air in Fig. 4.16. Similar to the midtropospheric case, dry air is generally shown to originate from the upper troposphere above 500 hPa. Most trajectories lead back to the Central/East Atlantic subtropics and midlatitudes in association with apparent anticyclones. A few originate over Africa and to the southeast but still from aloft (above the SAL). The source of dry air is not consistent with being of SAL origin, but rather with subsidence aloft in an anticyclone in most cases.

To examine the large-scale circulation pattern associated with the 300-500 hPa EOF1, 850 hPa heights with streamlines and 200-850 hPa vertical shear are examined in Figs. 4.17 and 4.18. The characteristics of the differences in the 850 hPa subtropical high in Fig. 4.14 are similar to what is observed for the 600-850 hPa layer except even more pronounced over the West Atlantic. The subtropical high is weaker over the West Atlantic or retreats eastward in the negative phase of the EOF1, which explains the increasing number of TCs that recurve northeastward over the Central Atlantic. The enhanced vertical shear off the coast of West Africa in the EOF1 positive phase contributes to the reduced

TC activity in that region, but the difference in the TC activity over the central MDR and the Gulf can not be explained by vertical shear.

Correlation analysis was conducted to examine the linkage between the upper level EOF1 and large-scale climate modes. A comparison between the upper and middle tropospheric correlations are shown in Figure 4.12. No significant correlations were found between the 300-500 hPa EOF1 and the AMM, NAO, or ENSO.

The correlation of the 300-500 hPa EOF1 pattern of dry air to Aug-Sep Atlantic precipitation was examined, and a significant correlation is present across the MDR, in particular between 15-20°N (not shown). Since it is collocated with the difference in the distribution of TC tracks between the positive and negative phases, the precipitation anomalies are partly due to the tropical cyclone activity. This negative correlation shows that, to the 95% confidence interval, the positive phase years of dry air events are associated with reduced precipitation. This is consistent with the notion that upper tropospheric dry air can act to suppress convection.

4.6 Summary

The interannual variability of the middle to upper tropospheric dry air and its impacts on Atlantic tropical cyclone activity were examined in this chapter. Relative humidity over the Atlantic in the middle troposphere displays a bimodal distribution (Brown and Zhang 1997), which reflects periods of drought and enhanced convective activity. In the upper troposphere, relative humidity is strongly skewed toward low values of RH. For this reason, it was necessary to define dry air occurrence on the synoptic time scale using the specific criteria: 1) relative humidity (RH) is equal to or less than half a standard deviation below the mean; 2) RH is less than a critical value (RHc); 3) conditions

1 and 2 are met continuously for one day. RHc is set to 50% for the middle troposphere and 40% for the upper troposphere.

The EOF analysis of dry air occurrence revealed a dominant mode of interannual variability with a center of action over the Central Atlantic for the middle (600-850 hPa) and upper (300-500 hPa) troposphere. Although the time series of the midtropospheric EOF1 is positively correlated to the upper tropospheric EOF1, the correlation coefficient (0.39) suggests that the two modes only explain a limited amount (~15%) of the total variance for each other, or the two modes are independent of each other to some extent.

The leading mode of EOF analysis (EOF1) based on the established dry air occurrence definition was examined to determine the role of dry events on TC activity. When midtropospheric dry air days occur more frequently (positive phase of EOF1), TC activity tends to be reduced over the MDR. Additionally, storm intensity tends to be higher for the negative phase years of the 600-850 hPa EOF leading mode, as evidenced by the increase in the number of major hurricanes in comparison to the positive phase. When the upper tropospheric dry air occurs more frequently, TC number is reduced by about 20%, especially in the central and eastern MDR, but more landfalling storms develop near the coast of Southeast US. Therefore, the middle and upper tropospheric dry air both affect TC activity but in a different way. The impacts of the upper tropospheric dryness are consistent with previous studies (Hopsch et al. 2010; Braun 2010; Fritz and Wang 2013; Hankes et al. 2014).

The possible sources of middle and upper tropospheric dry air were examined based on the two EOF modes. This analysis showed that enhanced DOD in the MDR is associated with a high frequency of occurrence of midtropospheric dry air but a reduced frequency of

occurrence of the upper tropospheric dry air. Furthermore, trajectory analysis shows that dry air in both the 600-850 hPa and 300-500 hPa layers originates from the upper troposphere over the East Atlantic in extratropical regions, as well as from West Africa. These results suggest that large-scale subsidence in association with anticyclonic flow, besides the SAL, is a significant dry air source and needs to be considered for the variability of Atlantic tropical cyclone activity.

The large-scale patterns and climate oscillations associated with the two EOF modes were also examined. An eastward retreated subtropical high in the negative phase of the 600-850 and 300-500 EOF1 patterns contributes to the increasing number of TCs that recurve northeastward over the Central Atlantic. For the 600-850 hPa EOF1, the difference in (VWS) can not explain the difference in TC activity over the eastern MDR region and the subtropical Atlantic (between 20-30N). The enhanced vertical shear off the coast of West Africa in the positive phase of the 300-500 hPa EOF1 contributes to reduced TC activity, but the vertical shear can not explain the variations of the TC activity over the Central MDR and the Gulf. The middle tropospheric air is correlated to the AMM, particularly on decadal time scales.

4.7 Figures

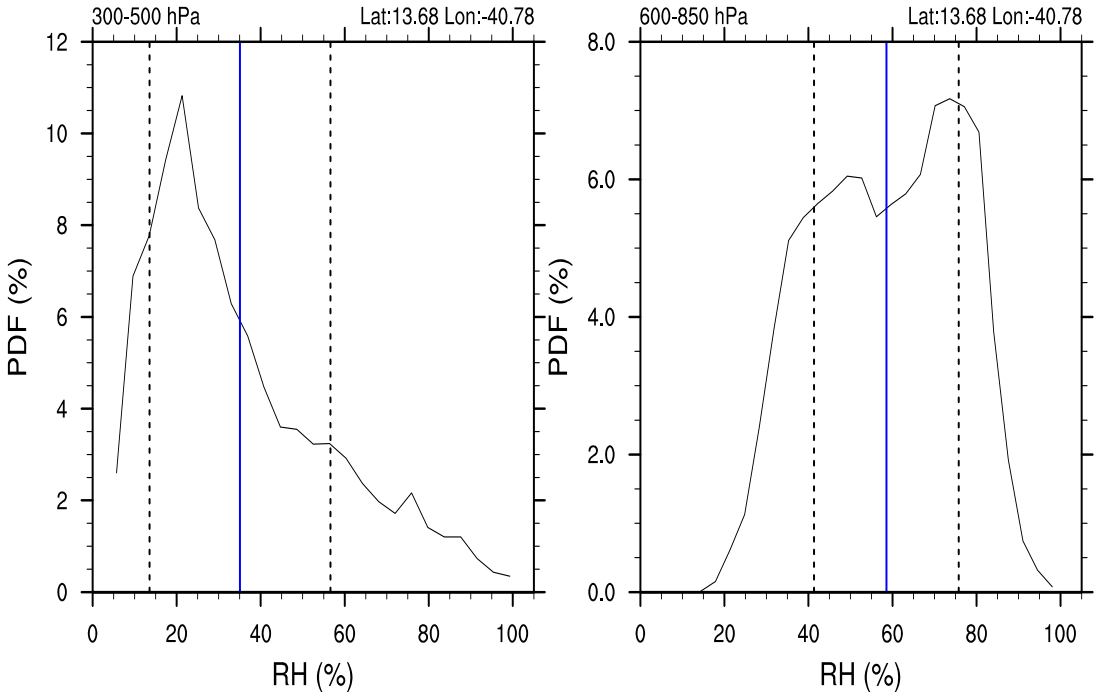

Figure 4.1 Probability distribution function of RH for 300-500 hPa (left) and 600-850 hPa (right). The mean RH for each layer is denoted by the blue line at this particular location, and the dashed line represents one standard deviation.

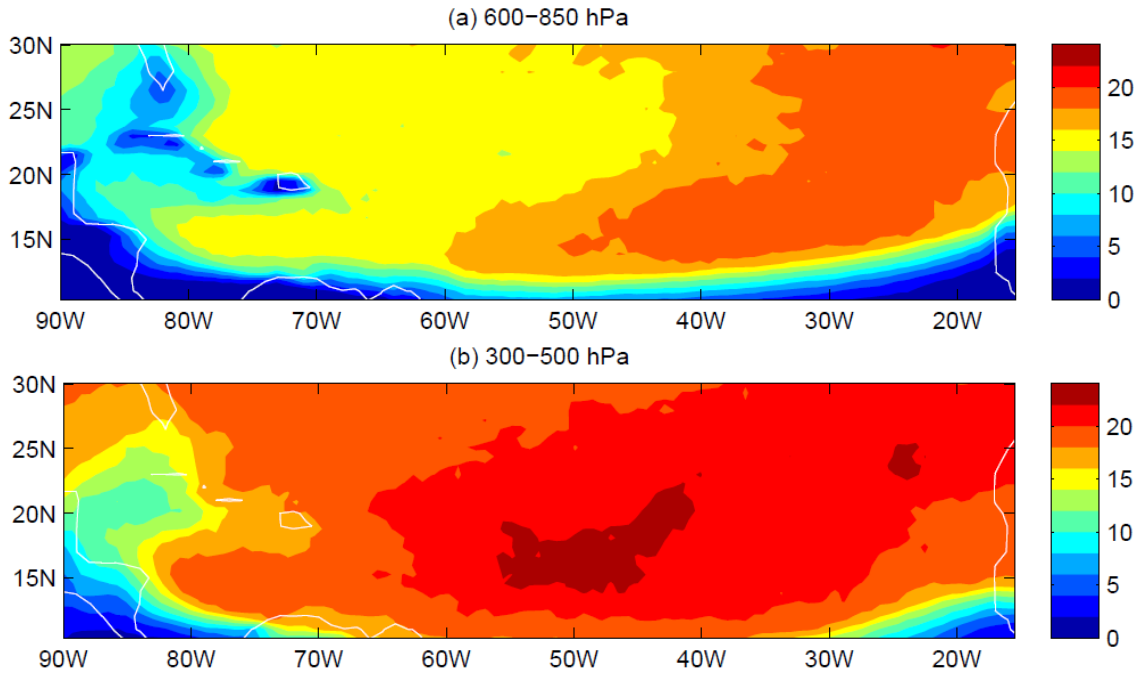

Figure 4.2 32-year average of dry event days (Aug-Sep) from 1979-2010.

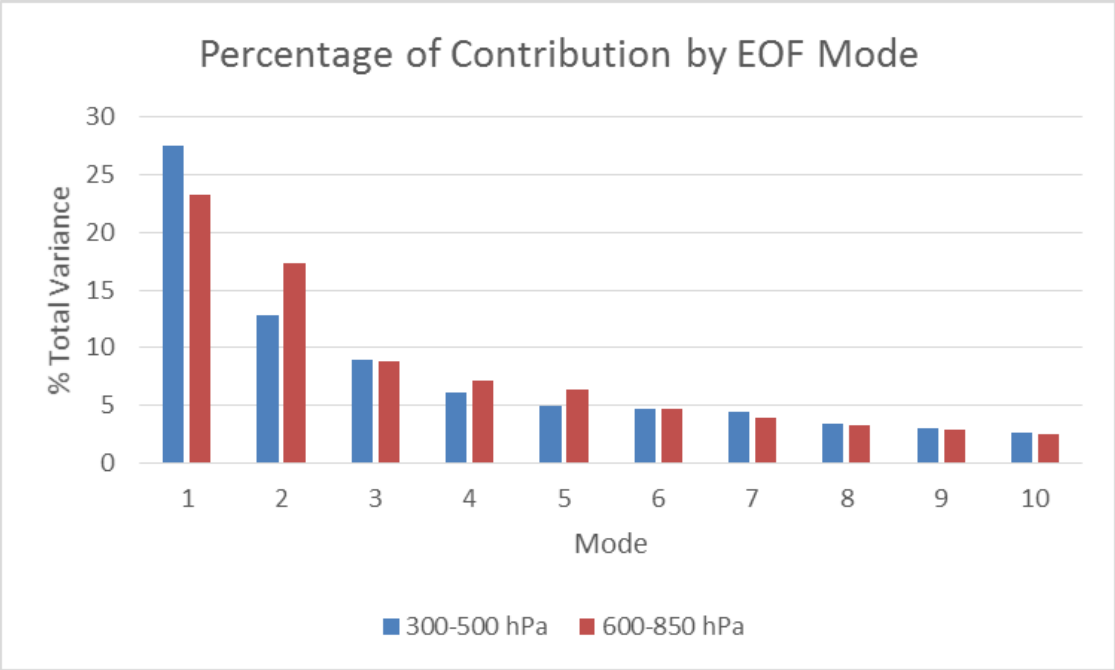

Figure 4.3 Contribution by the first 10 modes to the total variance of dry air occurrence from the 600-850 hPa and 300-500 hPa EOFs.

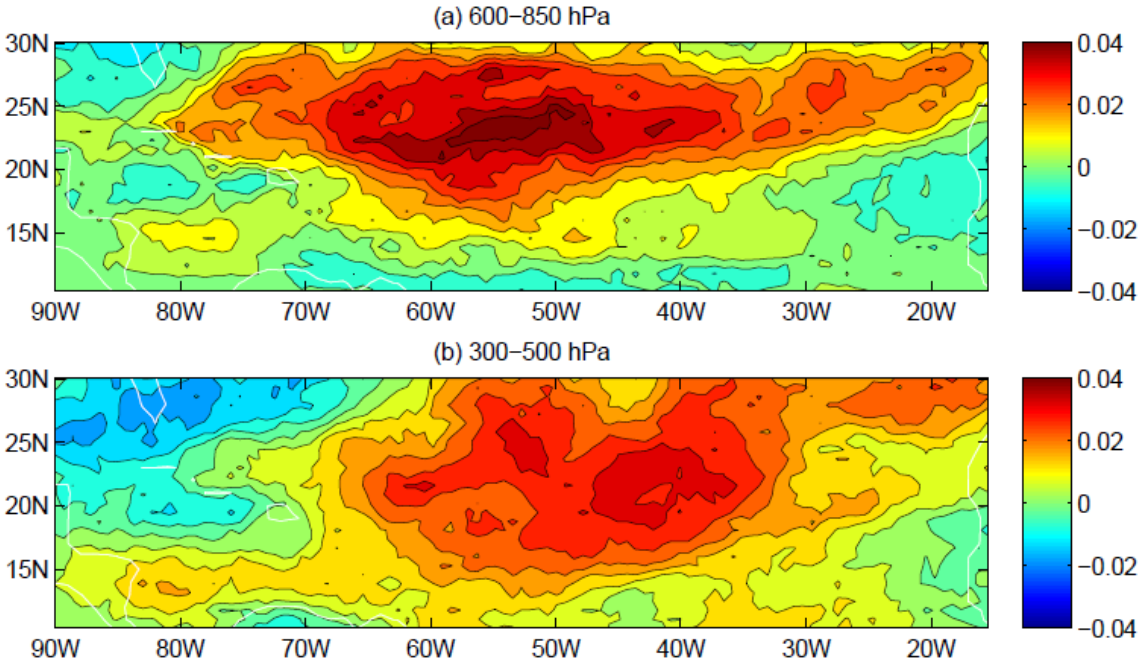

Figure 4.4 The First EOF Modes for the middle (top) and upper (bottom) troposphere. The correlation coefficient between these modes is .39, and the leading mode explains 23 (27) % of the variability in dry air occurrence for the middle (upper) troposphere.

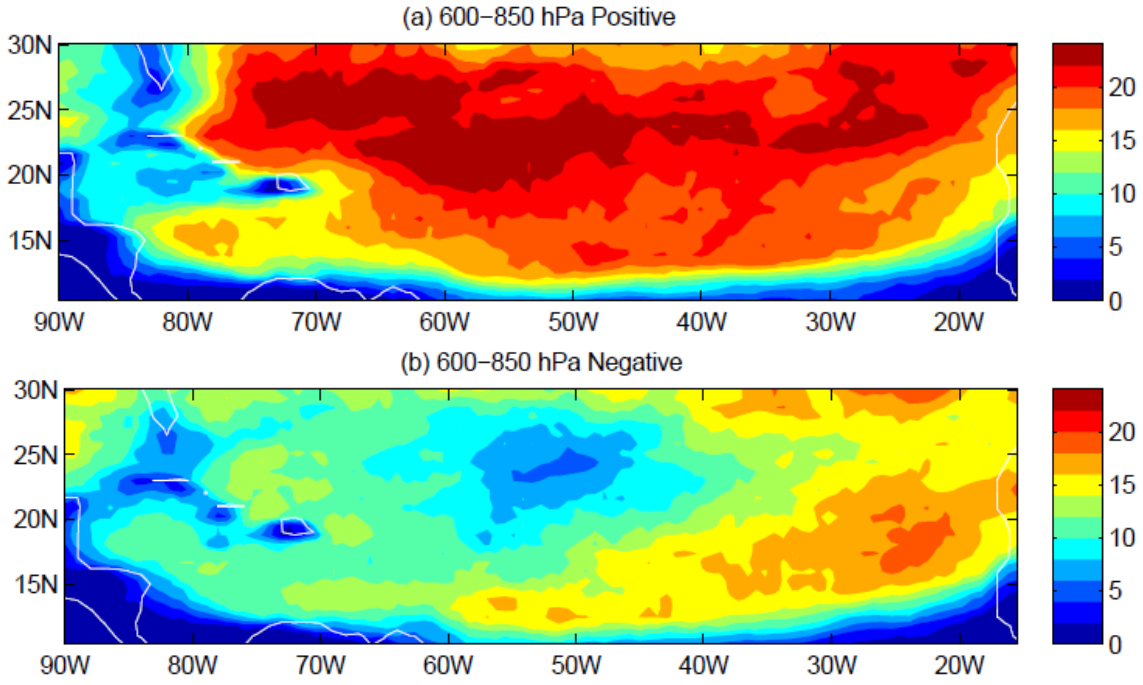

Figure 4.5 EOF1 (600-850): Dry air days for 6 most positive (a) and negative (b) years of the dry air event pattern.

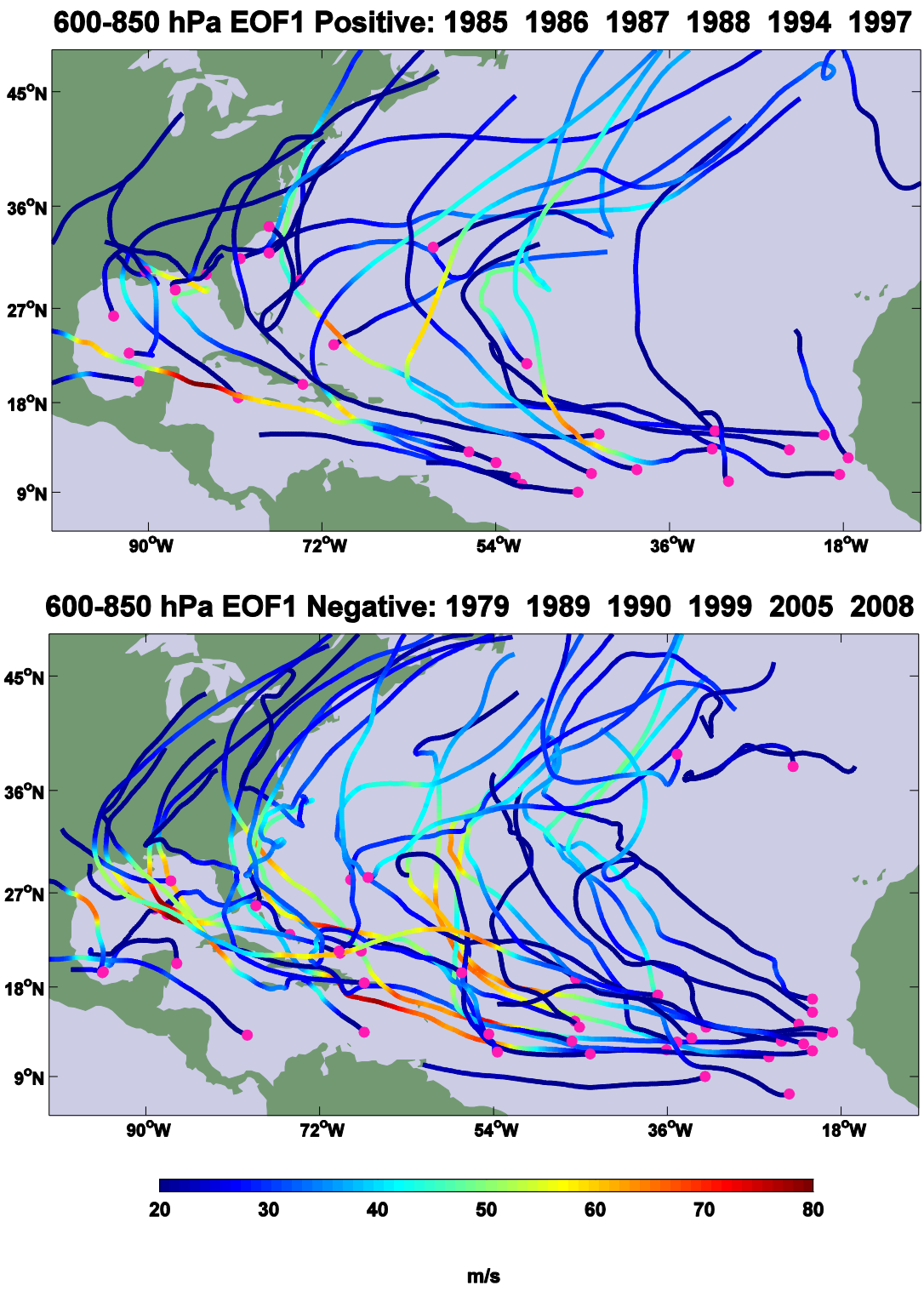

Figure 4.6 EOF1 (600-850): TC tracks for 6 most positive (top) and negative (bottom) years of the dry air event pattern. Shading represents TC intensity in m s^{-1}.

TC count	Middle EOF1	Upper EOF1
Pos	30	44
Neg	42	51
M Pos	6	12
M Neg	13	14

Figure 4.7 Number of named tropical cyclones in the positive (Pos) and negative (Neg) phases of the 600-850 (Middle) and 300-500 hPa (Upper) EOF1. Also included are the major (M) storms in Aug-Sep for the positive and negative phases of the EOFs.

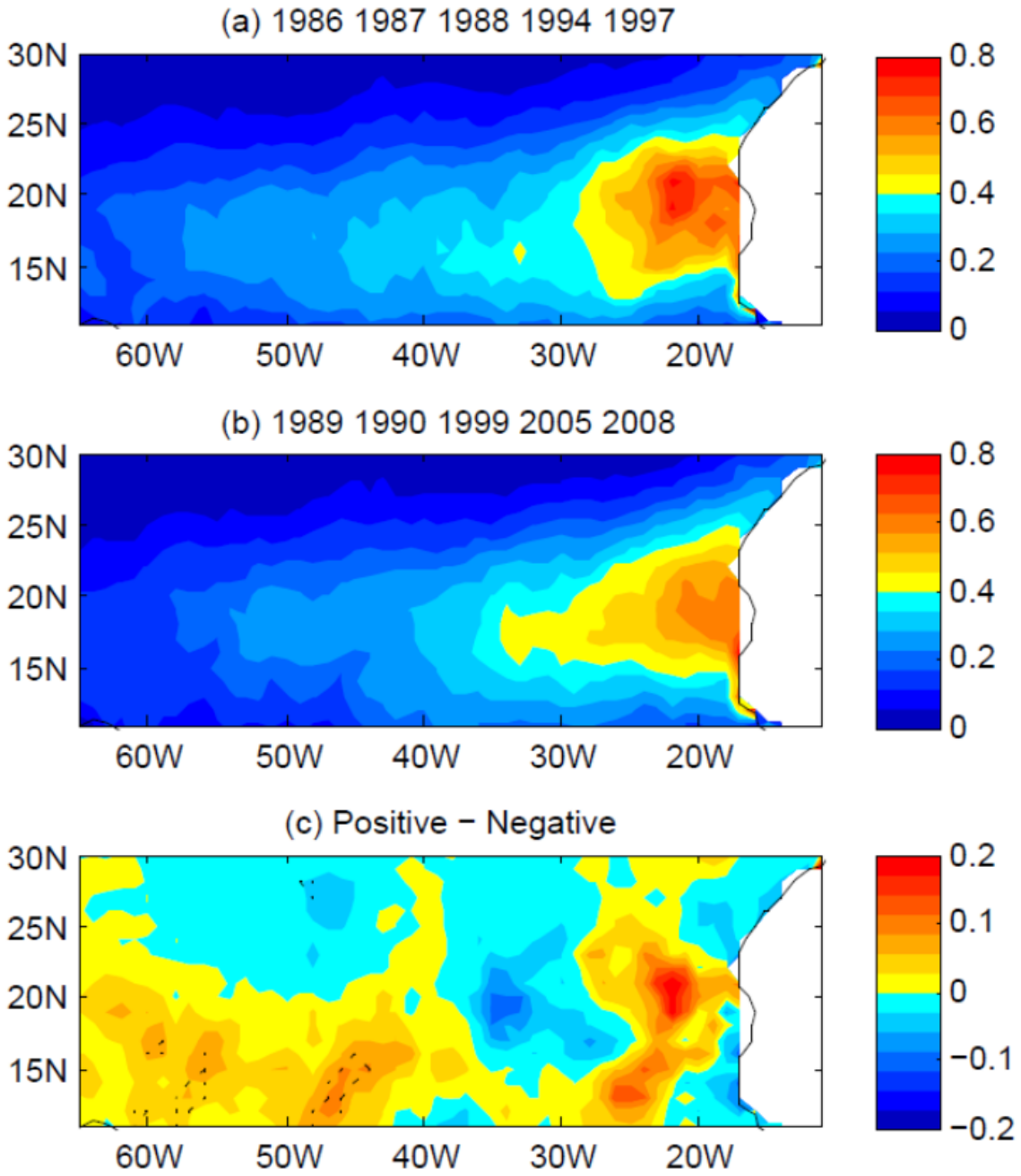

Figure 4.8 Composites of dust optical depth for the 5 strongest positive (a) and negative (b) phase years of the 600-850 hPa EOF leading mode. Dashed contours in the difference plot (c) represent statistical significance to the 95% confidence interval.

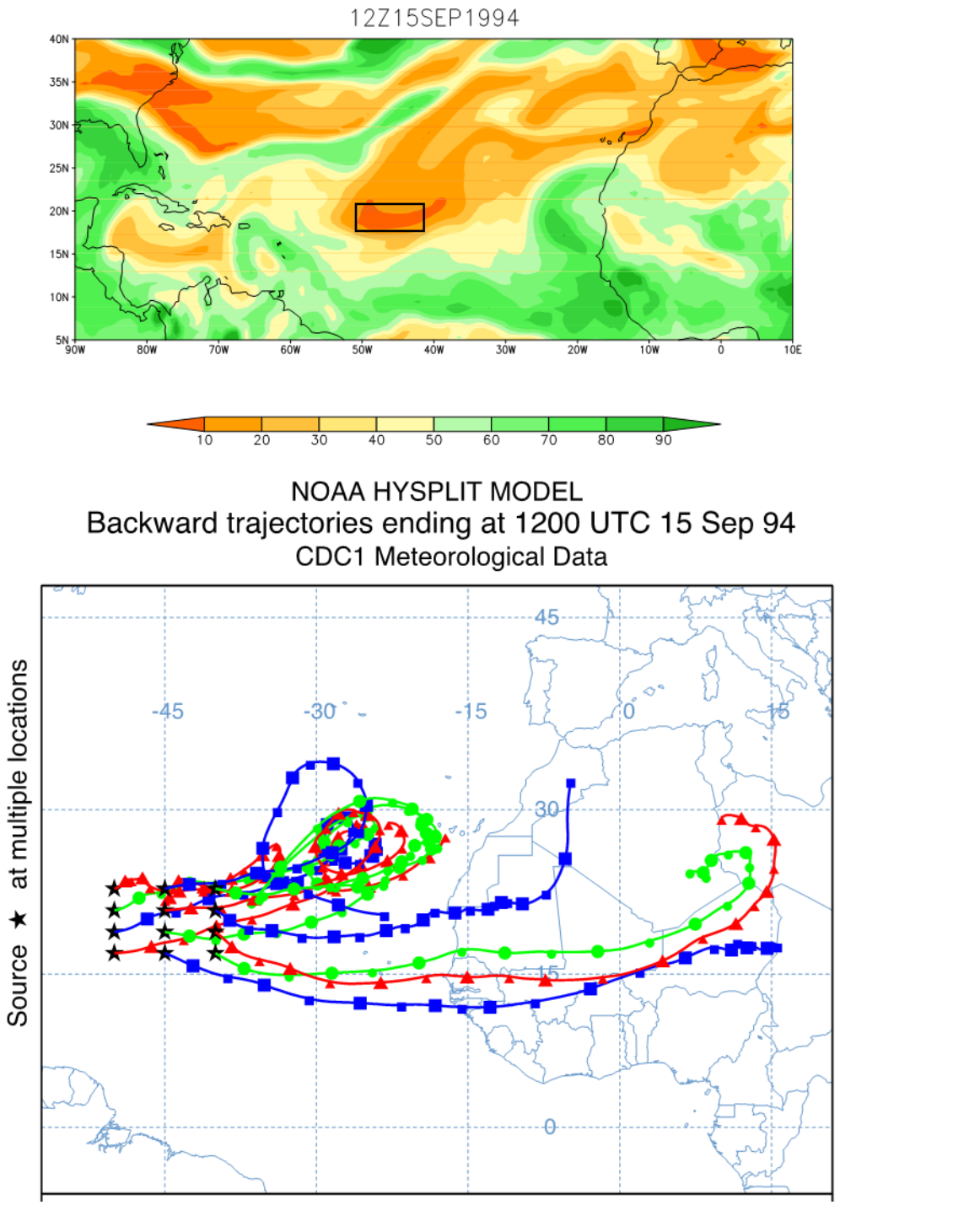

Figure 4.9 700 hPa RH from a representative dry air event for the 600-850 hPa EOF pattern (left). The box outlines a region within the core of the dry air from which trajectories were calculated. Ensemble of backward trajectories with the stars denoting the starting location and time from 699 hPa on 12Z 15-September, 1994 (right).

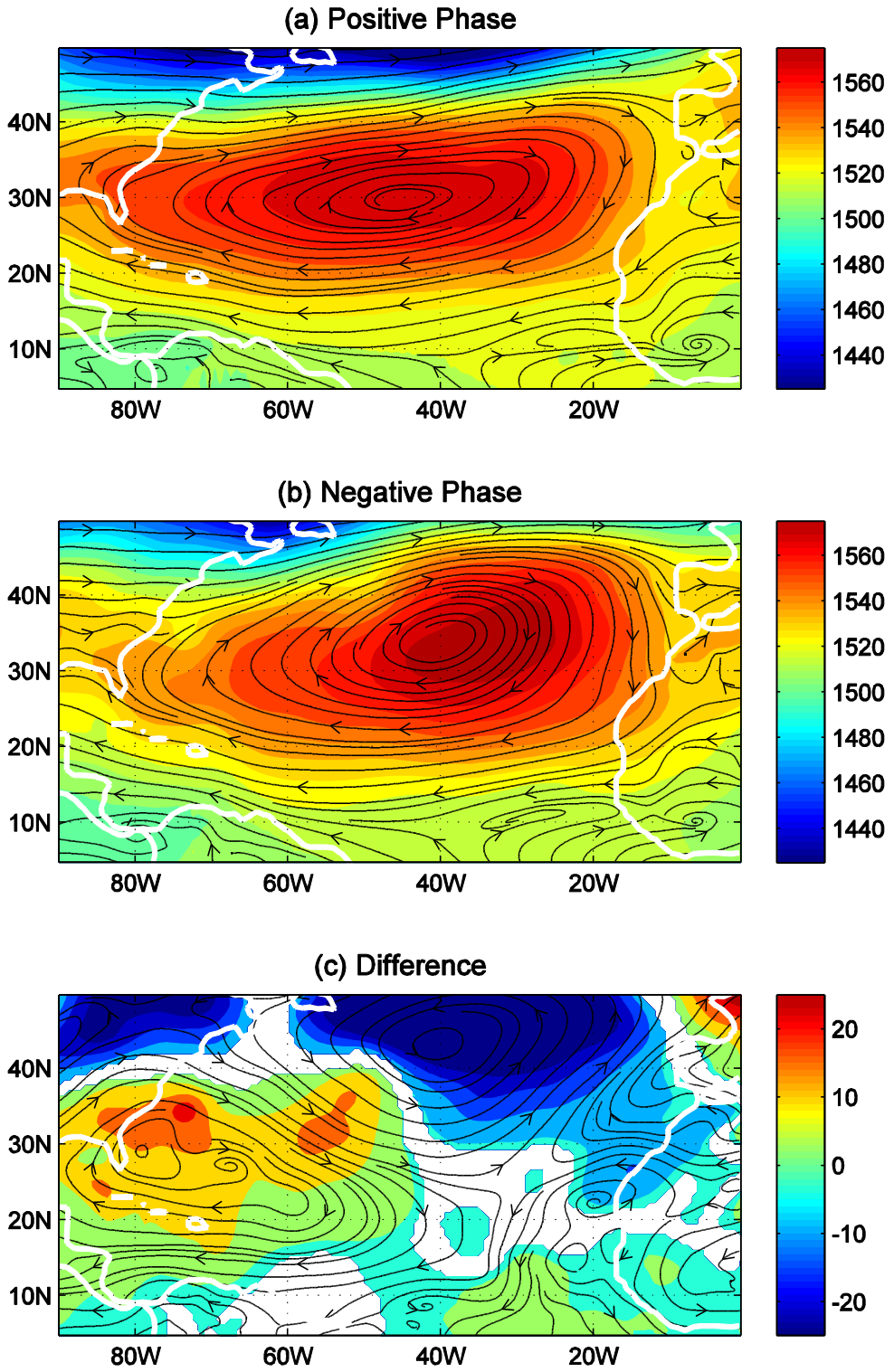

Figure 4.10 August-September 850 hPa heights (m) and UV streamlines for the 6 most positive (top) and negative (middle) years of the 600-850 hPa EOF1 pattern. The positive – negative phase differences are also plotted (bottom) for heights and streamlines. Only statistically significant differences to the 95% confidence interval are shown for heights.

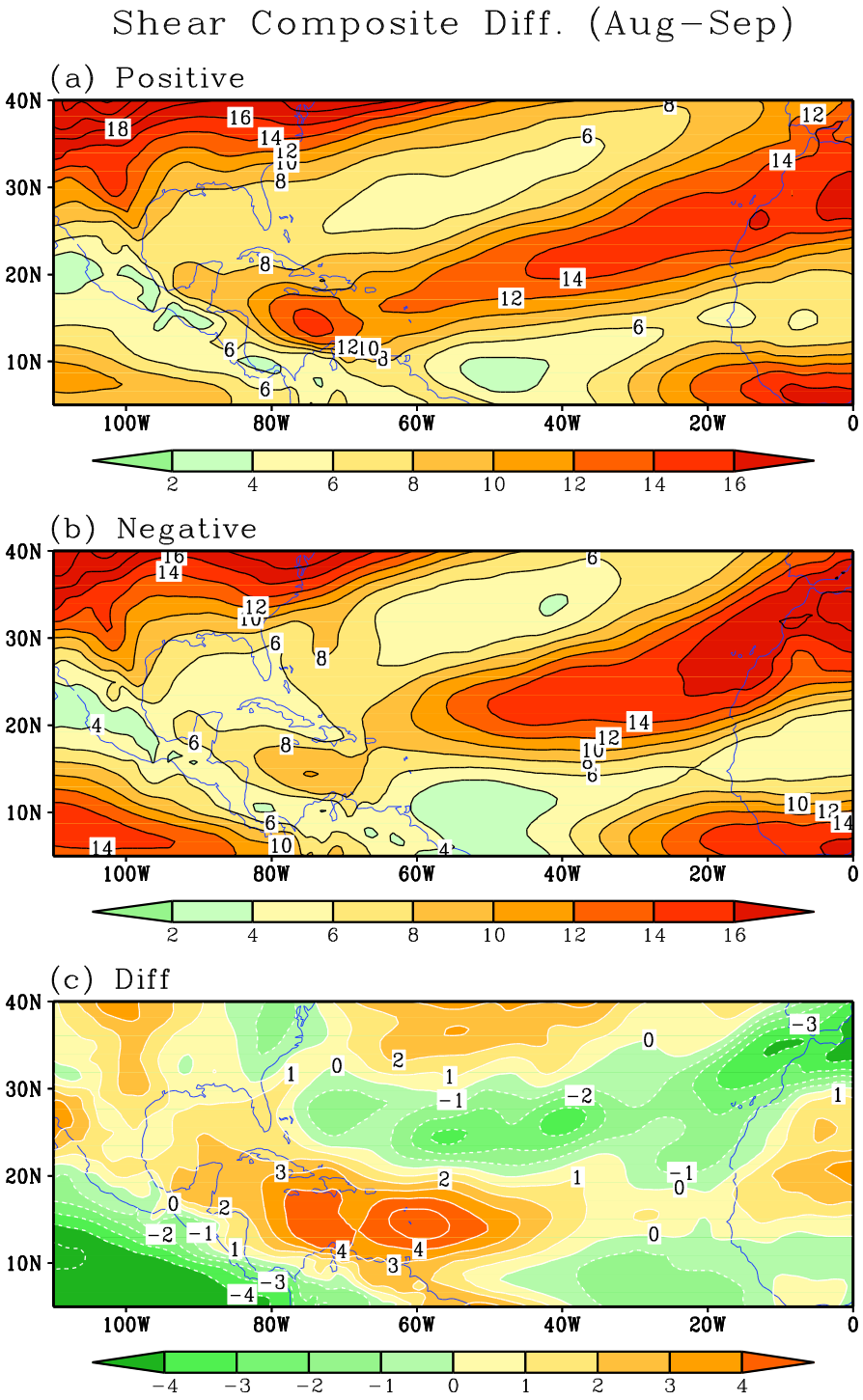

Figure 4.11 August-September 200-850 hPa vector shear (m s^{-1}) for the 6 most positive (a) and negative (b) years of the 600-850 hPa EOF1 pattern. The positive – negative phase differences are also plotted (c).

	AMM	ENSO	NAO
600-850 hPa EOF1	-0.4	0.17	-0.46
300-500 hPa EOF1	-0.02	0.19	-0.14

Figure 4.12 Correlations between 600-850 and 300-500 hPa EOF1 and various climate oscillations.

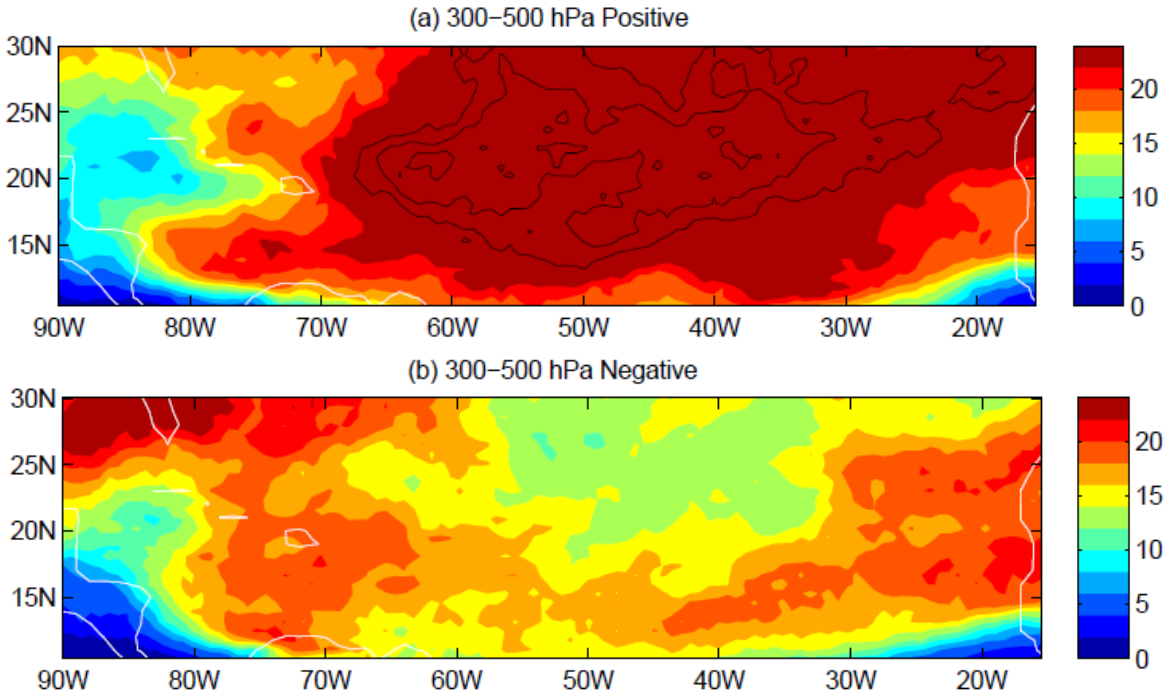

Figure 4.13 EOF1 (300-500): Dry air days for 6 most positive (a) and negative (b) years of the dry air event pattern. Black contours represent values of dry air days at 2 day intervals starting at 26.

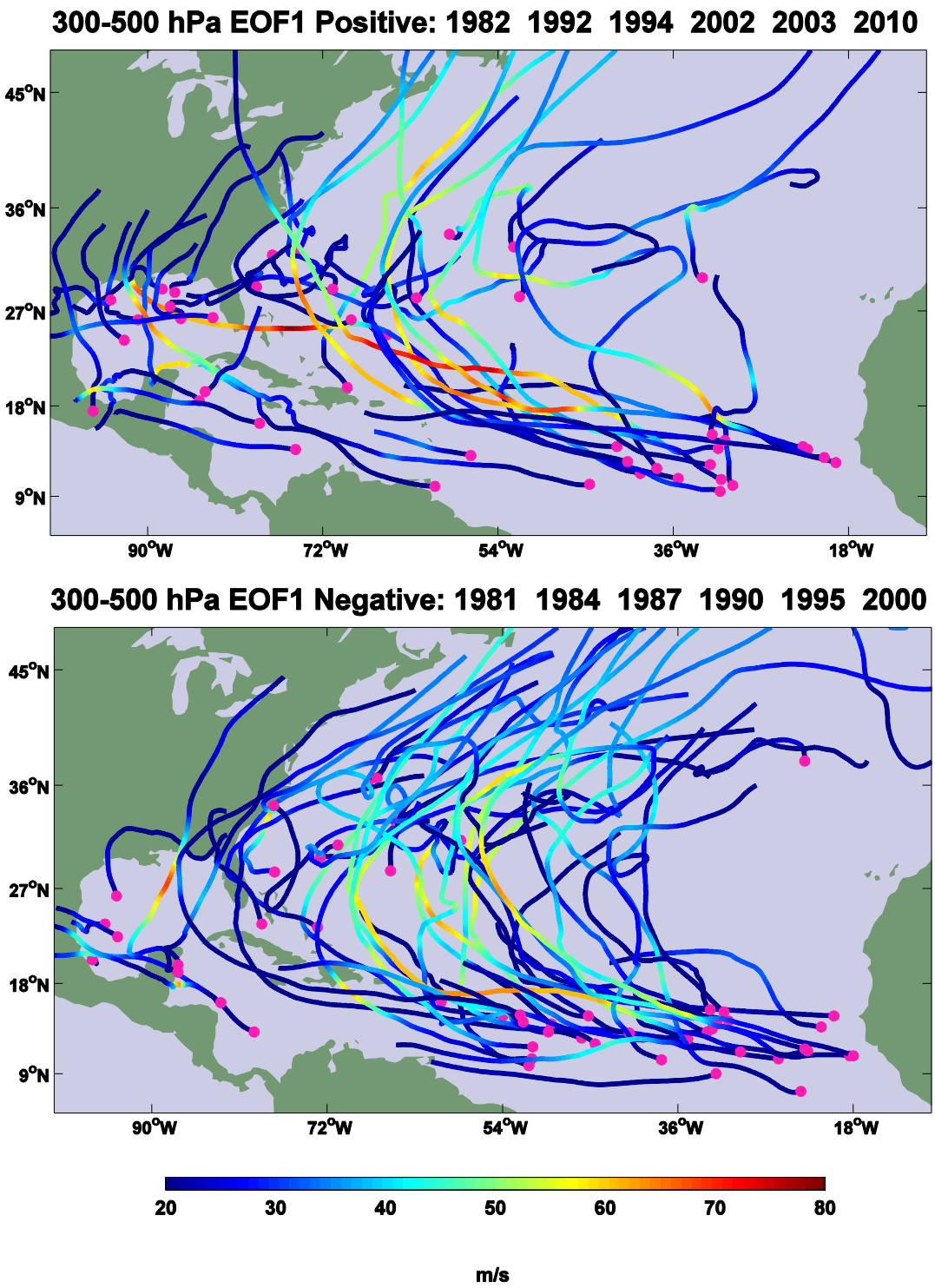

Figure 4.14 EOF1 (300-500 hPa): TC tracks for 6 most positive (top) and negative (bottom) years of the dry air event pattern.

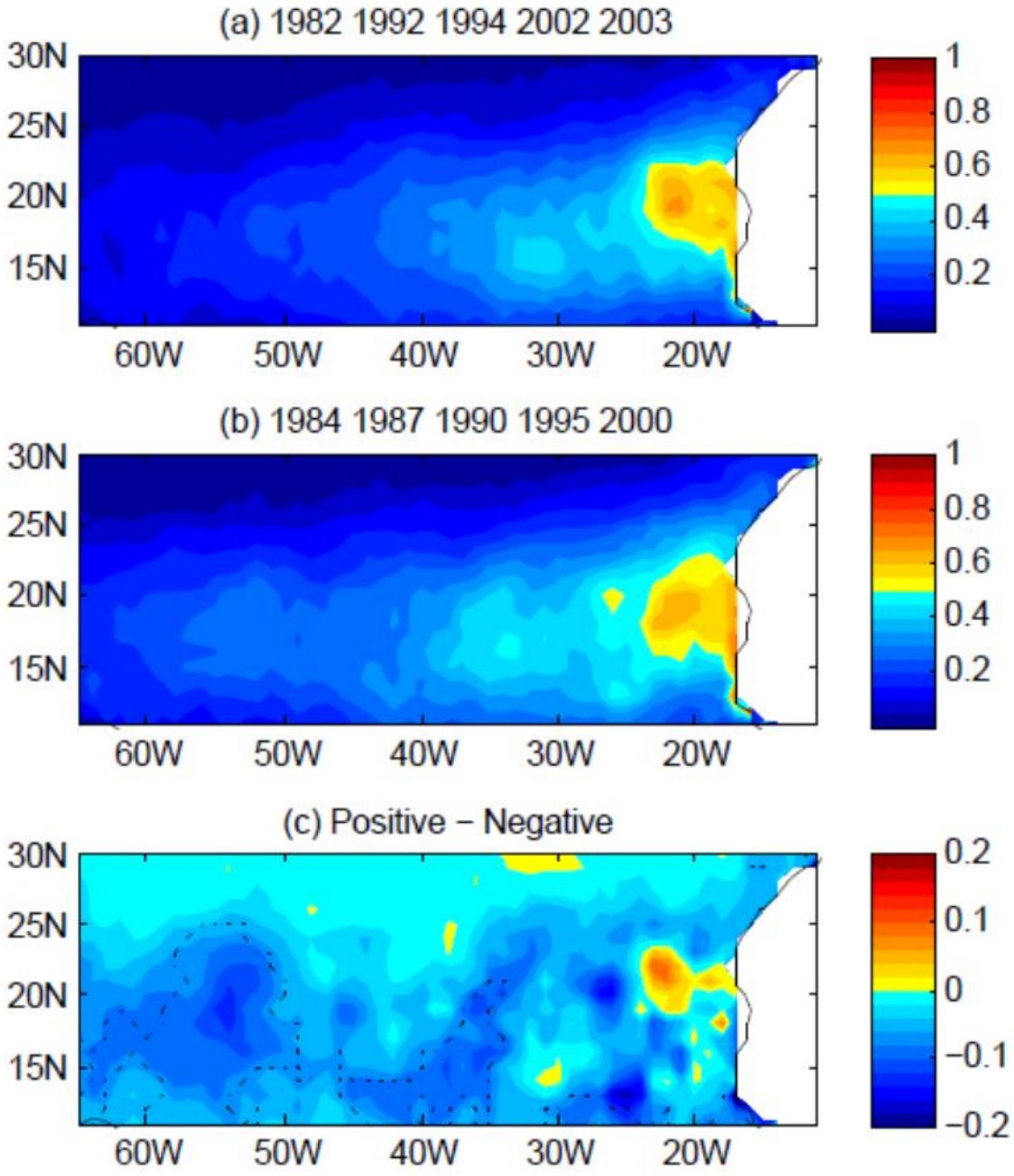

Figure 4.15 Composites of dust optical depth for the 5 strongest positive (a) and negative (b) phase years of the 300-500 hPa EOF leading mode. Dashed contours in the difference plot (c) represent statistical significance to the 95% confidence interval.

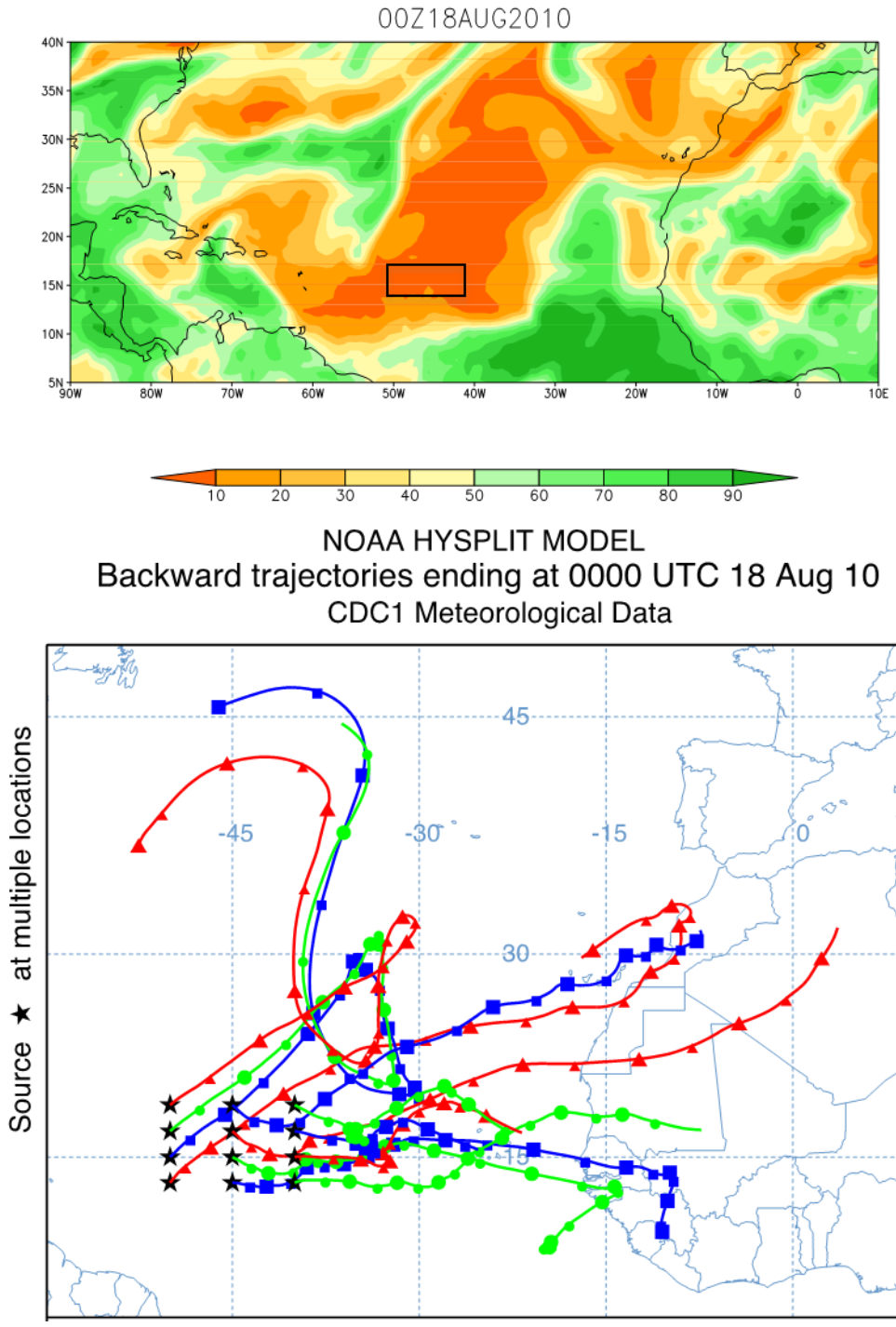

Figure 4.16 500 hPa RH from a representative dry air event for the 300-500 hPa EOF pattern (left). The box outlines a region within the core of the dry air from which trajectories were calculated. Ensemble of backward trajectories with the stars denoting the starting location and time from 699 hPa on 00Z 8-August, 2010 (right).

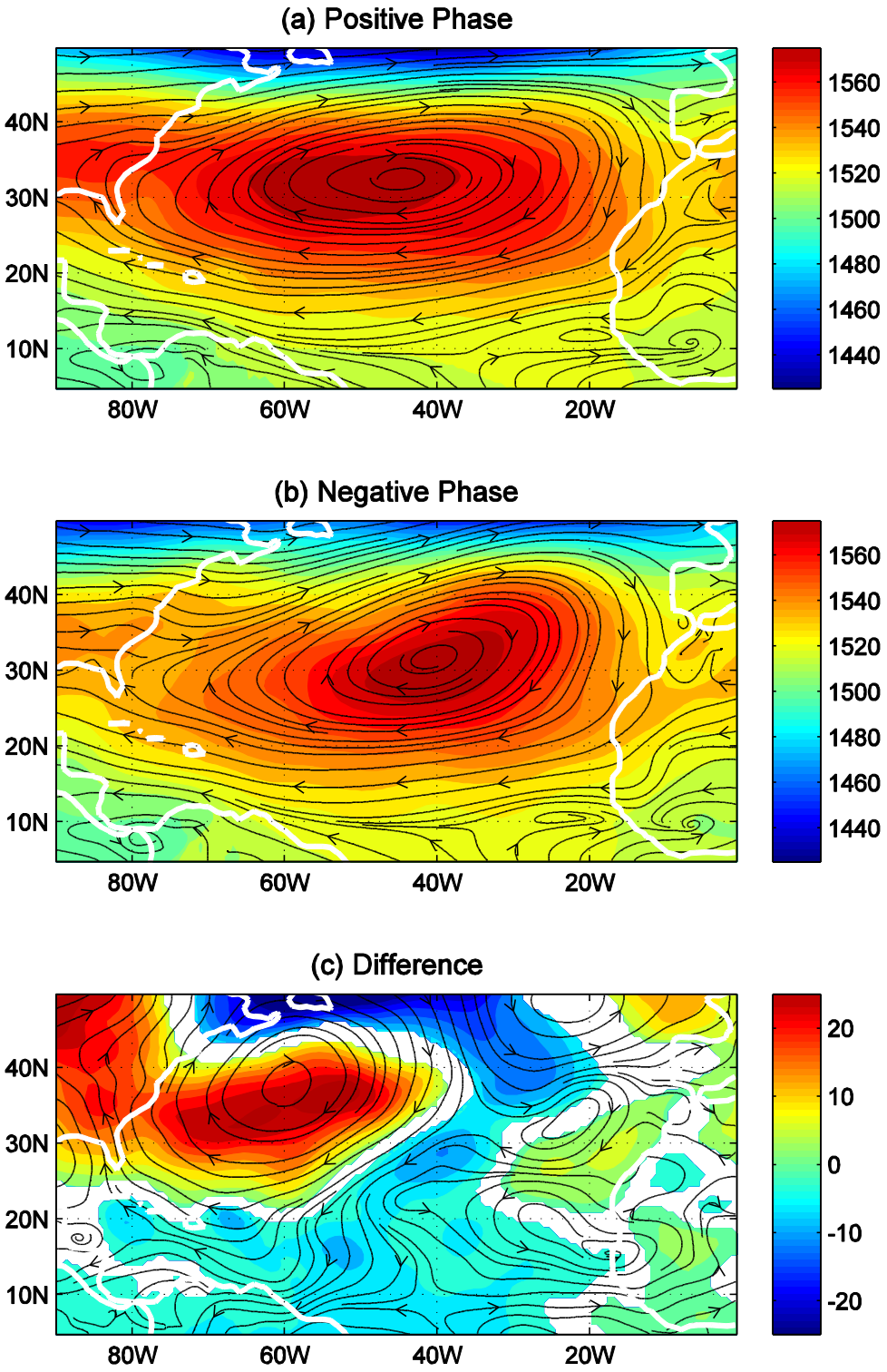

Figure 4.17 August-September 850 hPa heights (m) and UV streamlines for the 6 most positive (top) and negative (middle) years of the 300-500 hPa EOF1 pattern. The positive – negative phase differences are also plotted (bottom) for heights and streamlines. Only statistically significant differences to the 95% confidence interval are shown for heights.

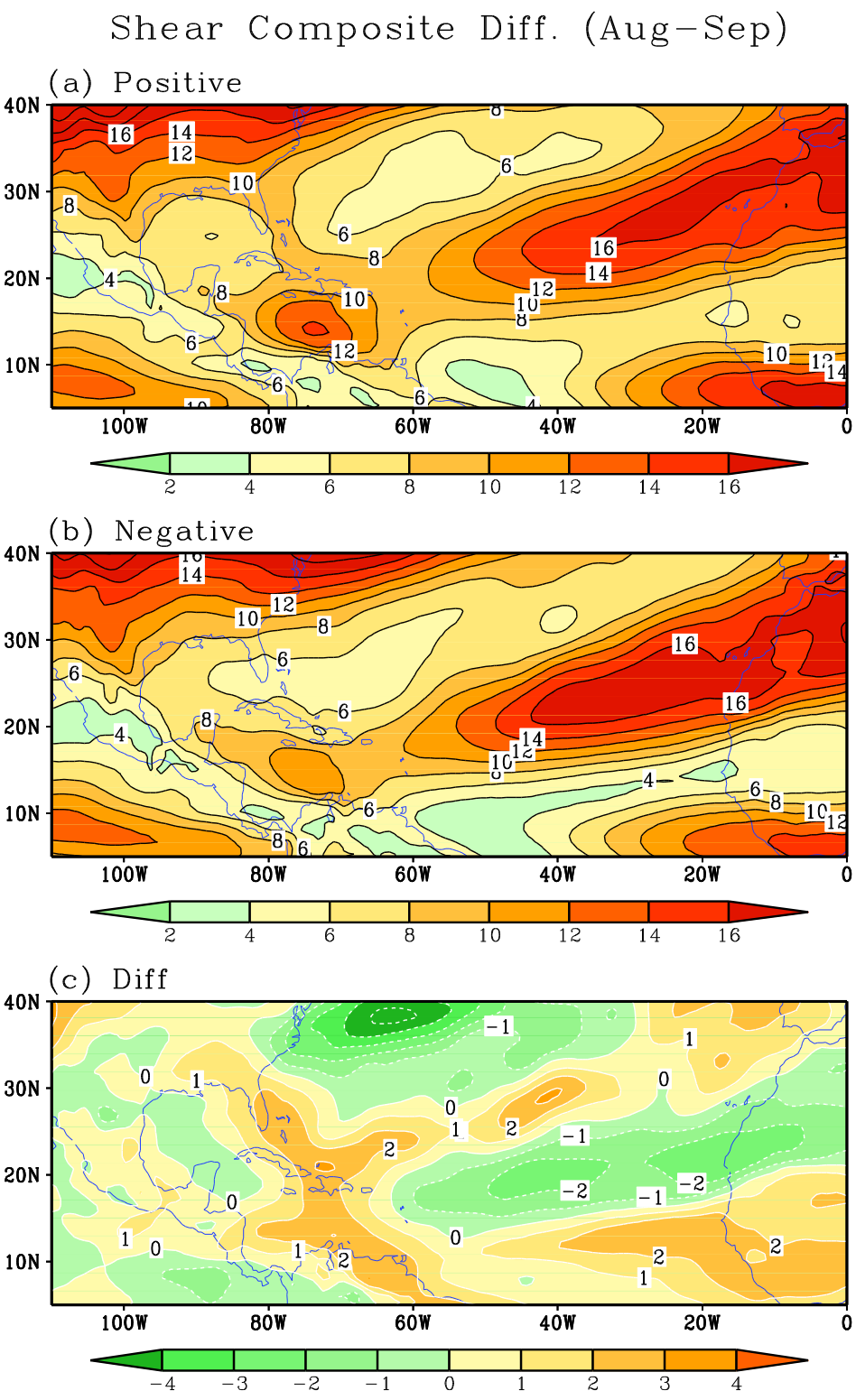

Figure 4.18 August-September 200-850 hPa UV vector shear (m s^{-1}) for the 6 most positive (a) and negative (b) years of the 300-500 hPa EOF1 pattern. The positive – negative phase differences are also plotted (c).

Chapter 5: Summary and Discussion

The pre-genesis evolution of wave pouches was examined for 164 named tropical cyclones over the Atlantic during 1989-2010 July-October using the ERA-Interim reanalysis and CMORPH precipitation. East of 60°W, most wave pouches (~80%) form at 700 hPa first, extending down to 850 or 925 hPa off the coast of West Africa. By contrast, the majority of the wave pouches (~68%) over the West Atlantic (west of 60°W) form at 850 or 925 hPa first. Wave pouches become more vertically aligned approaching genesis. It was also found that vorticity at 925 hPa intensifies faster than that at 600 hPa. A warm-core structure forms at the meso-β scale near the pouch center prior to genesis but is less well defined at the meso-α pouch scale. The evolution of precipitation and the low-level convergence suggests that convection begins to organize near the pouch center about one day prior to genesis, along with the rapid intensification of vorticity in the inner pouch region. The composites derived from the ERA-Interim reanalysis show that the inner pouch region has higher specific humidity and equivalent potential temperature, especially in the middle troposphere within one day prior to genesis.

This statistical analysis using the ERA-Interim revealed the different thermodynamic conditions and different vorticity evolution between the inner and outer pouch regions, and, along with the CMORPH data, suggests that the inner pouch region is the preferred location for sustained deep convection and tropical cyclogenesis, which supports the recent findings by Wang (2012) based on case studies. This study also shows that the ERA-Interim data can capture the meso-scale pouch structure to some extent.

While constructing the pouch tracks over the Atlantic in order to evaluate the inner and outer pouch regions, it was observed that a significant subset of 925 and 850 hPa waves

originated north of the AEJ over West Africa. Previous studies have identified two groups of waves over West Africa, one to the south and the other to the north of the African Easterly Jet (AEJ) (e.g., Reed et al. 1988; Pytharoulis and Thorncroft 1999; Thorncroft and Hodges 2001), which we were able to confirm from the perspective of the marsupial paradigm. The dynamic and thermodynamic evolution of the waves during the merger and the impacts of merger on the subsequent storm development are examined in this study. Three groups of storms are identified: non-merger developers, merger developers, and merger non-developers. Relative to non-merger developers, merger developers have a weaker circulation near the surface prior to merger, but the merger leads to a stronger and deeper wave pouch, which is more conducive to tropical cyclogenesis. Composite analysis shows that a merger developer is associated with a warmer and broader heat low over West Africa and a more extensive AEJ, which help to maintain the northern waves over the East Atlantic.

Merger developers and non-developers share a lot of characteristics at the early stages, but dry air intrusion west of the wave trough in the middle and upper troposphere inhibits deep convection and leads to the nondevelopment of some mergers. The dry air in non-developers is related to a strong and broad upper tropospheric trough and the associated subsidence west of the low-level wave pouch. The trough advects dry air from the extratropical Atlantic and also induces a strong westerly vertical shear. The composites of aerosol optical depth suggest that the Saharan Air Layer has a limited contribution to the dryness in the vicinity of the non-developers.

The finding about the impacts of the SAL on tropical cyclone formation is consistent with the recent studies by Braun (Braun 2010; Braun et al. 2012). Furthermore,

this study highlights the importance of the upper-level processes on tropical cyclone formation. Although the upper troposphere has low saturation specific humidity and can be moistened quickly by convection (Nolan 2007; Braun et al. 2012), the persistent presence of dry air due to strong vertical wind shear or large-scale subsidence can be detrimental to tropical cyclone formation (Fritz and Wang 2013).

Although this study examines only the Cape Verde storms, the investigation of the multi-disturbance interaction during tropical cyclone formation sheds light on tropical cyclone formation over the other basins. For example, tropical cyclone formation over the western North Pacific is often involved with the interaction of disturbances of different vertical structures and spatial scales, which is certainly a topic meriting further study. The role of dry air in the middle and upper troposphere may also have significance outside of Cape Verde storms.

To explore the impact of dry air on tropical cyclogenesis on a grander scale, we examined the interannual variability of dry air occurrence using relative humidity. The interannual variability of the frequency of the mid-tropospheric (600-850 hPa) and upper tropospheric (300-500) dry air occurrences and its impacts on tropical cyclone activity over the Atlantic are examined in this study. EOF analysis revealed a dominant mode of interannual variability of dry air layer frequency over the tropical north Atlantic, with strong variations over the western and central Atlantic between 15-30°N. It was found that middle tropospheric dry air impacts the TC number on interannual time scales, and also causes a reduction in the number of major hurricanes. 600-850 hPa dry air is associated with a strong SAL, but can also be shown to originate from higher latitudes in association with upper tropospheric anticyclones. Upper tropospheric dry air reduces TC number on

interannual time scales, but does not significantly impact storm intensity. 300-500 hPa dry air can not be attributed to the SAL, but rather is shown to originate from higher latitudes or West Africa typically in association with anticyclones.

The relationship of middle and upper tropospheric dry air occurrence as given by EOF analysis to the large-scale circulation and climate oscillations demonstrates the nature of its variability. The EOF1 positive phase for the 600-850 and 300-500 hPa layers is marked by a stronger subtropical high at 850 hPa that extends further westward to the West Atlantic. The steering flow and variations of vertical shear, besides the dry air occurrence, contribute to the variations of TC activity over the Atlantic to a degree. In the negative phase years of the EOF patterns, storms recurve over the Central Atlantic more frequently in association with a weakened and eastward retreated subtropical high. Therefore, the positive phase of the EOF1 patterns may be associated with fewer and weaker storms, but it is associated with a higher percentage of storms making landfall over North America. The variations of the TC activity can not be simply attributed to variations of vertical shear. This suggests that the middle and upper tropospheric dry air occurrence and the VWS both impact on TC activity. In terms of climate variability, the midtropospheric dry air occurrence is best correlated with the AMM and NAO, and the upper tropospheric dry air event frequency is correlated most strongly to precipitation, extending zonally from the Atlantic MDR.

The findings about the impacts of the dry air, especially the upper-level dry air, on tropical cyclone activity and the origin of dry air from the midlatitude suggests the importance of midlatitude processes on tropical cyclones. Further study is warranted on this topic to examine the potential for increased predictability of TC activity on the seasonal

time scales based on the teleconnections between the Atlantic humidity distribution and climate oscillations.

References

Arnault, J., and F. Roux, 2010: Comparison between Two Case Studies of Developing and NonDeveloping African Easterly Waves during NAMMA and AMMA/SOP-3: Absolute Vertical Vorticity Budget. *Mon. Wea. Rev.*, **138**, 1420-1445.

Aiyyer, A. R., and C. Thorncroft, 2006: Climatology of Vertical Wind Shear over the Tropical Atlantic. *J. Climate*, **19**, 2969-2983.

Berry, G. J., and C. Thorncroft, 2005: Case Study of an Intense African Easterly Wave. *Mon. Wea. Rev.*, **133**, 752-766.

Beven, J. and H. Cobb, 2004: Tropical cyclone report Hurricane Isabel. *http://www.nhc.noaa.gov/2003isabel.shtml.*

Braun, S. A., and Coauthors, 2013: NASA's Genesis and Rapid Intensification Processes (GRIP) Field Experiment. *Bull. Amer. Meteor. Soc.*, **94**, 345–363.

Braun, S. A., M. T. Montgomery, K.J. Mallen, and P.D. Reasor, 2010: Simulation and Interpretation of the Genesis of Tropical Storm Gert (2005) as Part of the NASA Tropical Cloud Systems and Processes Experiment. *J. Atmos. Sci.*, **67**, 999-1025.

Burpee, R. W., 1974: Characteristics of the North African easterly waves during the summers of 1968 and 1969. *J. Atmos. Sci.*, **31,** 1556– 1570.

Carlson, T., 1969: Some Remarks on African Disturbances and Their Progress Over the Tropical Atlantic. *Mon. Wea. Rev.*, **97**, 716-726.

Casey, S. P. F., A. E. Dessler, and C. Schumacher, 2009: Five-Year Climatology of Midtroposphere Dry Air Layers in Warm Tropical Ocean Regions as Viewed by AIRS/Aqua. *J. Appl. Meteorol.*, **48**, 1831-1842.

Chen, T. S., S. Y. Wang and A. J. Clark, 2008: North Atlantic Hurricanes Contributed by African Easterly Waves North and South of the African Easterly Jet. *J. Climate*, **21**, 6767-6776.

Cook, K. H., 1999: Generation of the African Easterly Jet and Its Role in Determining West African Precipitation. *J. Climate*, **12**, 1165-1184.

Davis, C. A., and D. A. Ahijevych, 2012: Mesoscale Structural Evolution of Three Tropical Weather Systems Observed during PREDICT. *J. Atmos. Sci.*, **69**, 1284-1305.

Davis, C. A., and D. A. Ahijevych, 2013: Thermodynamic Environments of Deep Convection in Atlantic Tropical Disturbances. *J. Atmos. Sci.*, **70**, 1912–1928.

Doblas-Reyes, F. J. and De´que´, M., 1998: A flexible bandpass filter design procedure applied to midlatitude intraseasonal variability, *Mon. Weather Rev.*, **126**, 3326-3335.

Draxler, R.R., and G.D. Hess, 1997: Description of the HYSPLIT_4 modeling system. NOAA Tech. Memo. ERL ARL-224, NOAA Air Resources Laboratory, Silver Spring, MD, 24 pp.

Draxler, R.R., and G.D. Hess, 1998: An overview of the HYSPLIT_4 modeling system of trajectories, dispersion, and deposition. *Aust. Meteor. Mag.*, **47**, 295-308.

Draxler, R.R., 1999: HYSPLIT4 user's guide. NOAA Tech. Memo. ERL ARL-230, NOAA Air Resources Laboratory, Silver Spring, MD.

Dunion, J. P., and C. S. Velden, 2004: The Impact of the Saharan Air Layer on Atlantic Tropical Cyclone Activity. *Bull. Amer. Meteor. Soc.*, 353-365.

Dunkerton, T. J., M. T. Montgomery, and Z. Wang, 2009: Tropical cyclogenesis in a

Tropical wave critical layer: Easterly waves. *Atmos. Chem. Phys*., **9**, 5587–5646.

Elsberry, R. L., and P. A. Harr, 2008: Tropical cyclone structure (TCS-08) field Experiment science basis, observational platforms, and strategy. *Asia-Pacific J. Atmos. Sci.*, **44**, 209-231.

Evan, A. T., A. K. Heidinger, and M. J. Pavolonis, 2006: Development of a new over-water Advanced Very High Resolution Radiometer dust detection algorithm. *Int. J. Remote Sens.*, **27**, 3903‐3924.

Evan, A. T., S. Mukhopadhyay, 2010: African Dust over the Northern Tropical Atlantic: 1955-2008. *J. Appl. Meteor. Climatol*., **49**, 2213–2229.

Fink, A. H., D. G. Vincent, P. M. Reiner, and P. Speth, 2004: Mean State and Wave Disturbances during Phases I, II, and III of GATE based on ERA-40. *Mon. Wea. Rev.*, **132**, 1661-1683.

Frank, N. L., 1970: Atlantic tropical systems of 1969. *Mon. Wea. Rev*., **98**, 307–314.

Fritz, C. and Z. Wang, 2013: A Numerical Study of the Impacts of Dry Air on Tropical Cyclone Formation: A Development Case and a Nondevelopment Case. *J. Atmos. Sci.*, **70**, 91-111.

Fu, B., M. S. Peng, T. Li, D. E. Stevens, 2012: Developing versus NonDeveloping Disturbances for Tropical Cyclone Formation. Part II: Western North Pacific. *Mon. Wea. Rev.*, **140**, 1067-1080.

Gray, W. M., 1968: Global view of the origin of tropical disturbances and storms. *Mon. Wea. Rev.*, **96**, 669–700.

Hall, N. M. J., G. N. Kiladis, and C. D. Thorncroft, 2006: Three-Dimensional Structure and Dynamics of African Easterly Waves. Part II: Dynamical Modes. *J. Atmos.*

Sci., **63**, 2231-2245.

Hankes, I., Z. Wang, G. Zhang, and C. Fritz, 2014: Impacts of East Atlantic Tropical Easterly Wave Mergers and Middle to Upper Tropospheric Dry Air on Tropical Cyclone Formation.

Hopsch, S. B., C. D. Thorncroft, K. Hodges, and A. Aiyyer, 2007: West African Storm Tracks and Their Relationship to Atlantic Tropical Cyclones. *J. Climate*, **20**, 2468-2483.

Hopsch, Thorncroft, and Tyle, 2010: Analysis of African Easterly Wave Structures and Their Role in Influencing Tropical Cyclogenesis. *Mon. Wea. Rev.*, **138**, 1399-1419.

Hubanks, P. A., M. D. King, S. A. Platnick, and R. A. Pincus, 2008: MODIS Atmosphere L3 Gridded Product Algorithm Theoretical Basis Document. ATBD Reference Number ATBD-MOD-30, 96 pp.

James, R. P., and P. M. Markowski, 2010: A Numerical Investigation of the Effects of Dry Air Aloft on Deep Convection. *Mon. Wea. Rev.*, **138**, 140-161.

Joyce, R. J., J. E. Janowiak, P. A. Arkin, and P. Xie, 2004: CMORPH: A method that Produces global precipitation estimates from passive microwave and infrared data at high spatial and temporal resolution. *J. Hydromet*., **5**, 487-503.

Karyampudi, V. M., J. Simpson, S. Palm, and H. Pierce, 1997: Lidar observations of Saharan dust layer and its influence on tropical cyclogenesis. Preprints, *22d Conf. on Hurricanes and Tropical Meteorology,* Fort Collins, CO, Amer. Meteor. Soc., 59–60.

Kerns, B., and E. Zipser, 2009: Four Years of Tropical ERA-40 Vorticity Maxima Tracks. Part II: Differences between Developing and Nondeveloping

Disturbances. *Mon. Wea. Rev.*, **137**, 2576-2591.

Kiladis, Thorncroft, and Hall, 2006: Three-Dimensional Structure and Dynamics of African Easterly Waves. Part I: Observations. *J. Atmos. Sci.*, **63**, 2212-2230.

Kilroy, G., and R. K. Smith, 2013: A numerical study of rotating convection during Tropical cyclogenesis. *Q. J. R. Meteorol. Soc.*, **139**, 1255-1269. DOI:10.1002/qj.2022

Landsea, C., 1993: A Climatology of Intense (or Major) Atlantic Hurricanes. *Mon. Wea. Rev.*, **121**, 1703-1713.

Liu, C. and E. J. Zipser, 2012: Regional variation of morphology of organized convection in the tropics and subtropics, *J. Geophys. Res*., doi:10.1029/2012JD018409.

Lucas, C., M. A. LeMone, and E. J. Zipser, 1996: Reply to Michaud, L.M., Comment on "Convective available potential energy in the environment of oceanic and Continental clouds". *J. Atmos, Sci*., **53**, 1212-1214.

Lussier, L., 2010. *A multi-scale analysis of tropical cyclogenesis within the critical layer Of tropical easterly waves in the Atlantic and western North Pacific sectors*. Ph.D. Naval Postgraduate School.

Mapes, B., and P. Zuidema, 1996: Radiative-Dynamical Consequences of Dry Tongues in the Tropical Troposphere. *J. Atmos. Sci*., **53**, 620-628.

McBride, J. L. and R. Zehr (1981): Observational Analysis of Tropical Cyclone Formation. Part II: Comparison of Non-Developing versus Developing Systems. *J. Atmos. Sci.*, **38**, 1132-1151.

Merrill, R. T., 1988: Environmental Influences on Hurricane Intensification. *J. Atmos. Sci.*, **45**, 1678-1687.

Molinari, J., D. Knight, M. Dickinson, D. Vollaro, and S. Skubis, 1997: Potential

Vorticity, Easterly Waves, and Eastern Pacific Tropical Cyclogenesis. *Mon. Wea. Rev.*, **125**, 2699-2708.

Montgomery, M. T., and Coauthors, 2012: The Pre-Depression Investigation of Cloud-Systems in the Tropics (PREDICT) Experiment: Scientific Basis, New Analysis Tools, and Some First Results. *Bull. Amer. Meteor. Soc.*, **93**, 153–172.

Montgomery, M.T., Z. Wang, and T. J. Dunkerton, 2010b: Coarse, intermediate and high resolution numerical simulations of the transition of a tropical wave critical layer to a tropical storm. *Atmos. Chem. Phys*., 10, 10 803–10 827.

Nitta, T., and Y. Takayabu, 1985: Global analysis of the lower tropospheric disturbances in the Tropics during the northern summer of the FGGE year. Part II: Regional characteristics of the disturbances. *Pure Appl. Geophys*., **123**, 272–292.

Nolan, D. S., 2007: What is the trigger for tropical cyclogenesis? *Aust. Meteorol. Mag.*, **56**, 241-266.Pytharoulis, I, and C. Thorncroft, 1999: The Low-Level Structure of African Easterly Waves in 1995. *Mon. Wea. Rev.*, **127**, 2266–2280.

Peng, M. S., B. Fu, T. Li, and D. E. Stevens, 2012: Developing versus NonDeveloping Disturbances For Tropical Cyclone Formation. Part I: North Atlantic. *Mon. Wea. Rev.*, **140**, 1047-1066.

Pytharoulis, I. and C. Thorncroft (1999): The Low-Level Structure of African Easterly Waves in 1995. *Mon. Wea. Rev.*, **127**, 2266-2280.

Raymond, D. J. and C. Lopez Carrillo, 2011: The vorticity budget of developing typhoon Nuri (2008), *Atmos. Chem. Phys*., **11**, 147-163.

Raymond, D. J., S. L. Sessions, and C. Lopez Carrillo, 2011: Thermodynamics of tropical

cyclogenesis in the northwest Pacific. *J. Geophys. Res*., **116**, D18101, doi:10.1029/2011JD015624.

Reed, R. J., D. C. Norquist, and E.E. Recker, 1977: The Structure and Properties of African Wave Disturbances as Observed During Phase III of GATE. *Mon. Wea. Rev.,* **105**, 317-333.

Reed, R. J., A. Hollingsworth, W. A. Heckley, and F. Delsol, 1988a: An Evaluation of the Performance of the ECMWF Operational System in Analyzing and Forecasting Easterly Wave Disturbances over Africa and the Tropical Atlantic. *Mon. Wea. Rev.,* **116**, 824-865.

Reed, R. J., M. D. Albright, A. J. Sammons, and P. Unden, 1988b: The Role of Latent Heat Release in Explosive Cyclogenesis: Three Examples Based on ECMWF Operational Forecasts. *Wea. Forecasting*, **3**, 217-229.

Ross, R. S., and T. N. Krishnamurti, 2007: Low-Level African Easterly Wave Activity and Its Relation to Atlantic Tropical Cyclogenesis in 2001. *Mon. Wea. Rev.*, **135**, 3950-3964.

Rozoff, Christopher M., Wayne H. Schubert, Brian D. McNoldy, James P. Kossin, 2006: Rapid Filamentation Zones in Intense Tropical Cyclones. *J. Atmos. Sci.*, **63**, 325–340.

Simmons, A.J., 1977: A Note on the Instability of the African Easterly Jet. *J. Atmos. Sci.*, **34**, 1670-1674.

Simmons, A, S. Uppala, D. Dee, and S. Kobayashi, 2007: ERA-Interim: New ECMWF reanalysis products from 1989 onwards. *Newsletter 110* - Winter 2006/07, ECMWF, 11 pp.

Thorncroft, C. D., D. J. Parker, R. R. Burton, M. Diop, J. H. Ayers, H. Bariat, S. Devereau, A. Diongue, R. Dumelow, D. R. Kindred, N. M. Price, M. Saloum, C. M. Taylor, and A. M. Tompkins, 2003: The JET2000 Project. *Bull. Amer. Meteor. Soc.*, 337-351.

Thorncroft, C., and K. Hodges, 2001: African Easterly Wave Variability and Its Relationship to Atlantic Tropical Cyclone Activity. *J. Climate*, **14**, 1166–1179.

Thorncroft, C., N. M. J. Hall, and G. N. Kiladis, 2008: Three-Dimensional Structure and Dynamics of African Easterly Waves. Part III: Genesis. *J. Atmos. Sci.*, **65**, 3596-3607.

Tory, K. J., R. A. Dare, N. E. Davidson, J. L. McBride and S. S. Chand, 2013: The importance of low-deformation vorticity in tropical cyclone formation. *Atmos. Chem. Phys.*, **13**, 2115-2132.

Tory, K. J., and W. M. Frank, 2010: Tropical cyclone formation. Global Perspectives on Tropical Cyclones, *2nd ed. J. Chan and J. D. Kepert, Eds*., World Scientific, 55–92.

Tuleya, R. E. and Y. Kurihara, 1981. A Numerical Study on the Effects of Environmental Flow on Tropical Storm Genesis. *Mon. Wea. Rev.*, **109**, 2487-2506.

Velden, C. S. and L. M. Leslie, 1991: The Basic Relationship between Tropical Cyclone Intensity and the Depth of the Environmental Steering Layer in the Australian Region. *Wea. Forecasting*, **6**, 244-253.

Vizy, E. K., and K. H. Cook, 2009: Tropical Storm Development from African Easterly Waves in the Eastern Atlantic: A Comparison of Two Successive Waves Using a Regional Model as Part of NASA AMMA 2006. *J. Atmos. Sci.*, **66**, 3313-3334.

Wang, Z., 2012: Thermodynamic Aspects of Tropical Cyclone Formation. *J. Atmos. Sci*., **69**, 2433-2451.

Wang, Z., 2014: Role of Cumulus Congestus in Tropical Cyclone Formation in a High Resolution Numerical Model Simulation. *J. Atmos. Sci.*, **0**, ( ) pp.

Wang, Z. and I. Hankes, 2014: Characteristics of Tropical Easterly Wave Pouches during Tropical Cyclone Formation. *Mon. Wea. Rev.*, **122**, 626-633.

Wang, Z., M. T. Montgomery, and T. J. Dunkerton, 2009: A dynamically-based method For forecasting tropical cyclogenesis location in the Atlantic sector using global Model products. *Geophys. Res. Lett*., **36**, L03801, doi:10.1029/2008GL035586.

Wang, Z., M. T. Montgomery, and T. J. Dunkerton, 2010a: Genesis of Pre–Hurricane Felix (2007). Part I: The Role of the Easterly Wave Critical Layer. *J. Atmos. Sci*., **67**, 1711–1729.

Wang, Z., M. T. Montgomery, and T. J. Dunkerton, 2010b: Genesis of Pre–Hurricane Felix (2007). Part II: Warm Core Formation, Precipitation Evolution, and Predictability. *J. Atmos. Sci*., **67**, 1730–1744.

Wang. Z., M. T. Montgomery, and C. Fritz, 2012: A First Look at the Structure of the Wave Pouch during the 2009 PREDICT–GRIP Dry Runs over the Atlantic. *Mon. Wea. Rev.*, **140**, 1144-1163.

Wentz, F. J. (2013), SSM/I Version-7 Calibration Report, report number 011012, Remote Sensing Systems, Santa Rosa, CA, 46 pp.

Wilks, D. S., 2006: Statistical Methods in the Atmospheric Sciences. *2d ed. Academic Press*, 648 pp.

Wu, L., H. Su, R. G. Fovell, B. Wang, J. T. Shen, B. H. Kahn, S. M. Hristova-Veleva, B.

H. Lambrigston, E. J. Fetzer, and J. H. Jiang, 2012: Relationship of environmental relative humidity with North Atlantic tropical cyclone intensity and intensification rate. *Geophys. Res. Lett.*, **39**, 1-8.

Yoneyama, K., and T. Fujitani, 1995: The behavior of dry westerly air associated with convection observed during the TOGA-COARE R/V Natushima cruise. *J. Meteor. Soc. Japan*, **73(2B)**, 291-304.

Yoneyama, K., and D. B. Parsons: A Proposed Mechanism for the Intrusion of Dry Air into the Tropical Western Pacific Region. *J. Atmos. Sci.*, **56**, 1524-1546.

Zawislak, J. and E. J. Zipser, 2010: Observations of Seven African Easterly Waves in the East Atlantic during 2006. *J. Atmos. Sci.*, **67**, 26-43.

Zhang, C., and M. D. Chou, 1999: Variability of Water Vapor, Infrared Radiative Cooling, and Atmospheric Instability for Deep Convection in the Equatorial Western Pacific. *J. Atmos. Sci.*, **56**, 711-723.

Zhang, C., and J. Pennington, 2004: African dry outbreaks. *J. Geopys. Res.*, **109**, D20108 13 pp.